



HAL
open science

Rhenium(I) Tricarbonyl Complexes of 1,10-Phenanthroline Derivatives with Unexpectedly High Cytotoxicity

Lucy E Enslin, Kallol Purkait, Maria Dalla Pozza, Bruno Saubamea, Pierre Mesdom, Hendrik G Visser, Gilles Gasser, Marietjie Schutte-Smith

► **To cite this version:**

Lucy E Enslin, Kallol Purkait, Maria Dalla Pozza, Bruno Saubamea, Pierre Mesdom, et al.. Rhenium(I) Tricarbonyl Complexes of 1,10-Phenanthroline Derivatives with Unexpectedly High Cytotoxicity. *Inorganic Chemistry*, 2023, 10.1021/acs.inorgchem.3c00730 . hal-04170566

HAL Id: hal-04170566

<https://hal.science/hal-04170566>

Submitted on 25 Jul 2023

HAL is a multi-disciplinary open access archive for the deposit and dissemination of scientific research documents, whether they are published or not. The documents may come from teaching and research institutions in France or abroad, or from public or private research centers.

L'archive ouverte pluridisciplinaire **HAL**, est destinée au dépôt et à la diffusion de documents scientifiques de niveau recherche, publiés ou non, émanant des établissements d'enseignement et de recherche français ou étrangers, des laboratoires publics ou privés.

Rhenium(I) Tricarbonyl Complexes of 1,10 Phenanthroline Derivatives with Unexpectedly High Cytotoxicity

*Lucy E. Enslin,^{a,#} Kallol Purkait,^{b,#} Maria Dalla Pozza,^b Bruno Saubamea,^c Pierre Mesdom,^b
Hendrik G. Visser,^{a*} Gilles Gasser^{b*} and Marietjie Schutte-Smith^{a*}*

^a University of the Free State, Department of Chemistry, Bloemfontein, 9301, South Africa.

^b Chimie ParisTech, PSL University, CNRS, Institute of Chemistry for Life and Health Sciences, Laboratory for Inorganic Chemical Biology, F-75005 Paris, France.

^c Université de Paris, Plateforme Imagerie Cellulaire et Moléculaire, F-75270 Paris, France

[#] these authors have contributed equally to the work.

* schuttem@ufs.ac.za

KEYWORDS: Bioorganometallic Chemistry; Cancer; Medicinal Inorganic Chemistry; Metals in Medicine; Rhenium.

Abstract

Eight rhenium(I) tricarbonyl aqua complexes with the general formula *fac*-[Re(CO)₃(*N,N'*-bid)H₂O][NO₃] (**1-8**), where *N,N'*-bid is 2,6-dimethoxypyridyl)imidazo[4,5-*f*]1,10-phenanthroline (**L1**), (indole)imidazo[4,5-*f*]1,10-phenanthroline (**L2**), (5-methoxyindole)-imidazo[4,5-*f*]1,10-phenanthroline (**L3**), (biphenyl)-imidazo[4,5-*f*]1,10-phenanthroline (**L4**), (fluorene)imidazo[4,5-*f*]1,10-phenanthroline (**L5**), (benzo[*b*]thiophene)imidazo[4,5-*f*]1,10-phenanthroline (**L6**), (5-bromothiazole)imidazo[4,5-*f*]1,10-phenanthroline (**L7**), and (4,5-dimethylthiophene)imidazo[4,5-*f*]1,10-phenanthroline (**L8**), were synthesized and characterized using ¹H and ¹³C{¹H} NMR, FT-IR, UV/Vis absorption spectroscopy and ESI-mass spectrometry and their purity checked by elemental analysis. The stability of the complexes in aqueous buffer solution (pH 7.4) was confirmed by UV/Vis spectroscopy. The cytotoxicity of the complexes (**1-8**) was then evaluated on prostate cancer cells (PC3), showing a low nanomolar to low micromolar *in vitro* cytotoxicity. Worthy of note, three of the Re(I) tricarbonyl complexes showed very low (IC₅₀ = 30-50 nM) cytotoxic activity against PC3 cells and up to 26-fold selectivity over normal human retinal pigment epithelial-1 (RPE-1) cells. The cytotoxicity of both complexes **3** and **6** was lowered under hypoxic conditions in PC3 cells. However, the compounds were still 10 times more active than cisplatin in these conditions. Additional biological experiments were then performed on the most selective complexes (complexes **3** and **6**). Cell fractioning experiments followed by ICP-MS studies revealed that **3** and **6** accumulate mostly in the mitochondria and nucleus, respectively. Despite the respective mitochondrial and nuclear localization of **3** and **6**, **3** did not trigger the apoptosis pathways for cell killing, whereas **6** can trigger apoptosis but not as a major pathway. Complex **3** induced a paraptosis pathway for cell killing while **6** did not induce any of our other tested pathways, namely necrosis, paraptosis and autophagy. Both complexes **3** and **6** were found

to be involved in mitochondrial dysfunction and downregulated the ATP production of PC3 cells. To the best of our knowledge, this report presents some of the most cytotoxic Re(I) carbonyl complexes with exceptionally low nanomolar cytotoxic activity toward prostate cancer cells, demonstrating further the future viability of utilizing rhenium in the fight against cancer.

Introduction

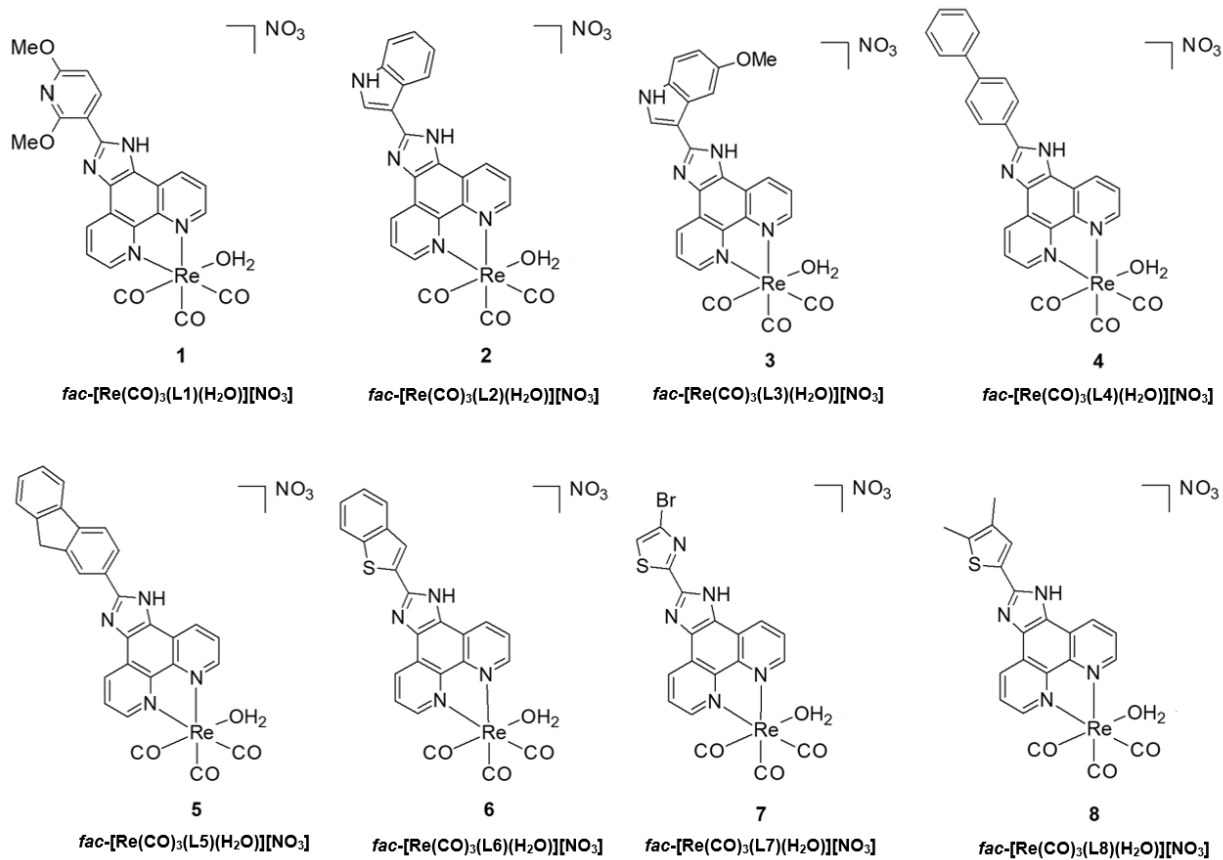
Rhenium(I) tricarbonyl complexes are attractive due to a number of potential applications. These include, but are not limited to photophysics,^{1,2} artificial photosynthetic materials,^{3,4,5} supramolecular systems,^{6,7,8} electrocatalysis,^{9,10} photoinduced catalysis^{9,10} and nuclear medicine.^{11,12} For decades, organometallic compounds have proven to be auspicious anti-cancer drug candidates,^{13,14,15,16,17} as such complexes may afford diverse mechanisms of action. Rhenium organometallic compounds display several innate properties, such as large Stokes shifts, long-lived emission states, emission tunability through ligand variation, and high quantum yields. These characteristics allow simplified elucidation of the mechanism of action and the cellular distribution of the compounds through emission spectroscopy. Due to their ability to chelate with metal ions such as *N,N'*-donor bidentate ligands, imidazole-phenanthroline derivatives play a vital role in biochemistry, analytical chemistry, and electrochemistry.^{18,19,20,21,22,23} Several synthetic polycyclic compounds of the type $[M(L,L')_2]^{n+}$, where M is a transition metal ion and L,L' an imidazo-phenanthroline type ligand have been reported to successfully interact with DNA.^{24,25}

An essential requirement of cancer treatments is the ability to induce cancer cell death whilst preserving the life of healthy non-cancerous cells. In recent studies, the use of rhenium(I) tricarbonyl complexes as possible anti-cancer agents have shown promising results.^{26,27,28,29,30,31} Wang *et al.* reported rhenium(I) tricarbonyl complexes with the ability to exert irreversible oxidative stress as well as glutathione metabolism disorder by means of accumulating in the mitochondria.³² A rhenium isonitrile complex reported by Wilson *et al.* induces apoptosis by means of unfolded protein response and additionally shows *in vitro* and *in vivo* anti-cancer activity toward ovarian cancer cells.^{33,34} Furthermore, they reported the scaffold protein NUBP2 that are involved in Fe-S cluster biogenesis, as a relevant target for a Re(I) complex (TRIP).³⁵ Simpson *et al.* designed rhenium(I) complexes that have the ability to induce cell death by means of the

inhibition of the phosphorylation of Aurora-A kinase.³⁶ Delasoie *et al.* reported a Re(I) tricarbonyl complex that exhibited selectivity toward HCT-116 cells,³⁷ while Ye *et al.* reported a rhenium(I)-based histone deacetylase inhibitor with the ability to target mitochondria as well as suppress histone deacetylases activity.³⁸

The development of anti-cancer agents that exhibit numerous mechanisms of action is of great importance, since such compounds may have the ability to overcome typical obstacles such as ineffectiveness toward tumours and drug resistance.^{39,40} A promising strategy in drug development to increase the potential of anti-cancer drugs in exhibiting multiple mechanisms of action, is the coordination of organic molecules with anti-cancer potential, to various metals. With this in mind and the recent success of imidazo[4,5-*f*]1,10-phenanthroline derivatives as prospective anti-cancer agents in colorectal and liver cancer,^{41,42,43} we designed a small library of rhenium(I) tricarbonyl complexes (Figure 1) with *N,N'*-bidentate imidazo[4,5-*f*]1,10-phenanthroline derivative ligand systems, with systematic changes with N, S and aromatic motifs on the backbone, having an appended aqua ligand to evaluate their potentials as anticancer agents. Rhenium(I) tricarbonyl complexes are usually kinetically inert which will help increasing the complex half-life to reach the target. The aqua ligand will further increase the possibility of target binding.⁴⁴ The deprotonation of the metal bonded labile aqua ligand and DNA binding ability of the complexes were investigated. Furthermore, we carried out *in vitro* cytotoxicity studies against prostate cancer and normal cells to obtain a small structure-activity relationship (SAR). The cellular localization, cellular uptake pathways and possible cell killing pathways of the complexes was also studied.

Figure 1. Chemical structures of rhenium(I) tricarbonyl complexes **1 - 8**.



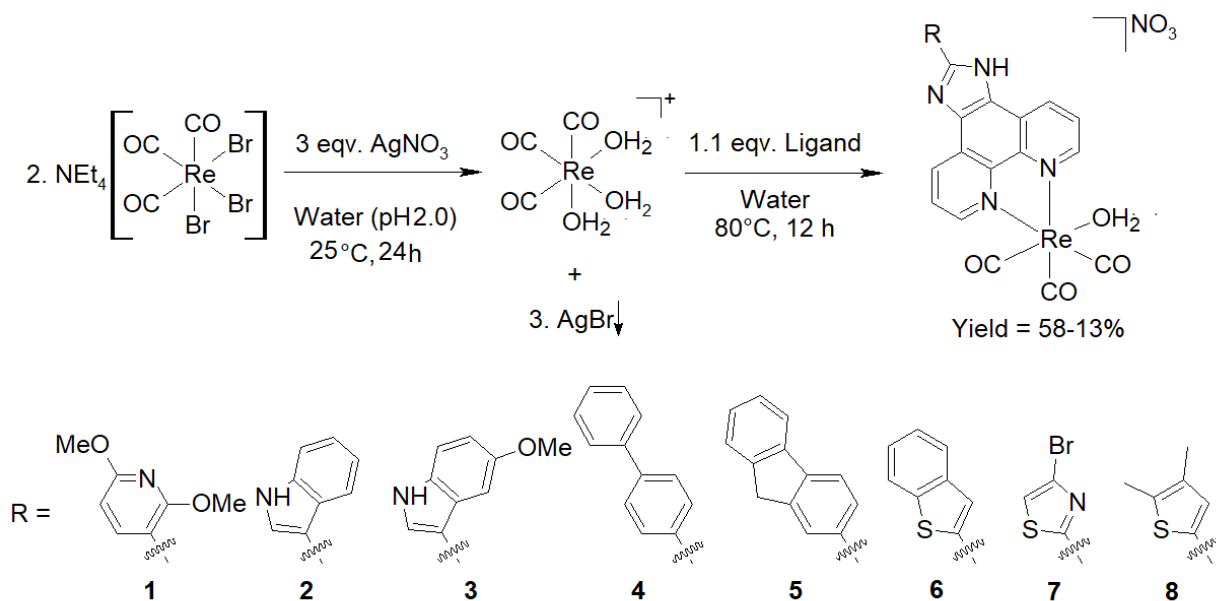
Results and Discussion

Synthesis and Characterisation

The procedure reported by Alberto *et al.* was utilised for the synthesis of the rhenium(I) carbonyl complexes starting synthon, $fac-[NEt_4]_2[Re(CO)_3(Br)_3]$ (ReAA)⁴⁵. The characteristic CO stretching frequencies of ReAA were observed at 1864 and 1998 cm^{-1} , respectively. The three Br⁻ ligands were replaced by labile aqua ligation *via* the addition of $AgNO_3$ at pH 2, resulting in the intermediate $fac-[Re(CO)_3(H_2O)_3][NO_3]$ compound. Water is a good leaving group and can thus be effortlessly replaced by other ligands. Complexes **1** - **8** were obtained by the addition of the respective N-N bidentate ligands viz., (2,6-dimethoxyphenyl)imidazo[4,5-*f*]1,10-phenanthroline (**L1**), (indole)imidazo[4,5-*f*]1,10-phenanthroline (**L2**), (5-methoxyindole)imidazo[4,5-*f*]1,10-

phenanthroline (**L3**) (biphenyl)imidazo[4,5-*f*]1,10-phenanthroline (**L4**), (fluorene)imidazo[4,5-*f*]1,10-phenanthroline (**L5**), (benzo[*b*]thiophene)imidazo[4,5-*f*]1,10-phenanthroline (**L6**), (5-bromothiazole)imidazo[4,5-*f*]1,10-phenanthroline (**L7**), and (4,5-dimethylthiophene)imidazo[4,5-*f*]1,10-phenanthroline (**L8**), respectively, to the acidic *fac*-[Re(CO)₃(H₂O)₃][NO₃] solution, producing the *fac*-[Re(CO)₃(*N,N'*-bid)(H₂O)][NO₃] type compounds. The general synthetic procedure for **1** – **8** is illustrated in Scheme 1. All compounds were characterized using ¹H and ¹³C{¹H} NMR, FT-IR, UV/Vis absorption spectroscopy and ESI-mass spectrometry and their purity checked by elemental analysis.

Scheme 1. General synthetic procedure for compounds **1** – **8**.



X-ray Crystallography

fac-[Re(CO)₃(L3)(Br)] (**3a**) was grown from a solution of *fac*-[Re(CO)₃(L3)(H₂O)][NO₃] and NEt₄Br in DMSO. The aqua complex did not yield any suitable crystals, however, upon

substitution of the axial aqua ligand with a bromido ligand, crystals suitable for single crystal crystallography were obtained. The crystallographic data for **3a** is summarised in Table S1 and the molecular diagram of the crystal structure is given in Figure 2. *fac*-[Re(CO)₃(L3)(Br)] (**3a**) crystallised in the triclinic $P\bar{1}$ space group, with one molecule and one solvent dimethyl sulfoxide molecule in the asymmetric unit. The bond distances and angles of **3a** are in range with similar structures and are reported in Table 1.^{46,47,48,49,50,51,52,53}

Figure 2. Molecular representation of the crystal structure of *fac*-[Re^I(CO)₃(L3)(Br)].DMSO (**3a**). Hydrogen atoms (except two N-H) are omitted for clarity and ellipsoids are drawn at 50 % probability level.

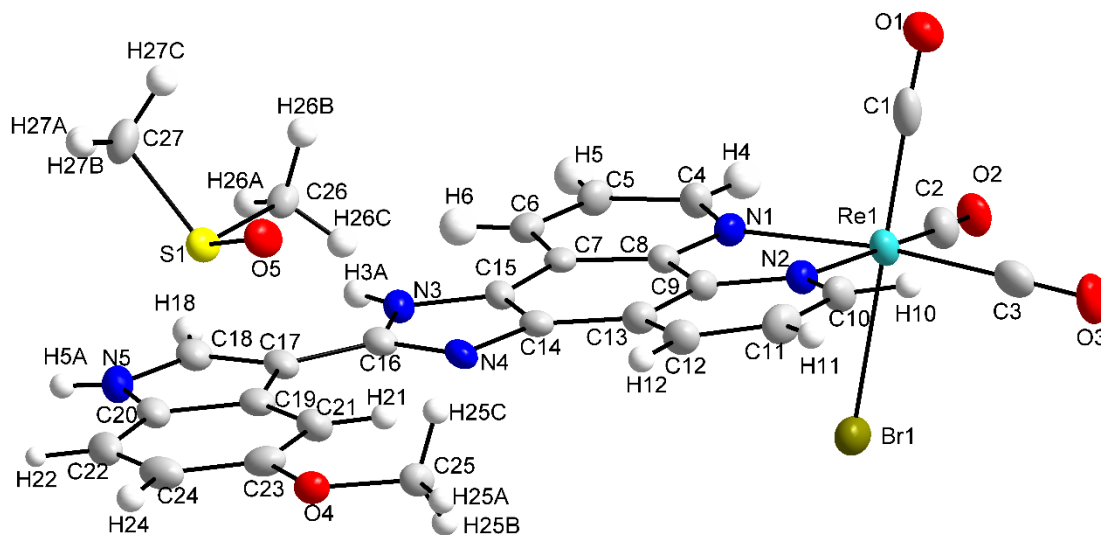


Table 1. Selected bond distances and angles (Å, °) of **3a**.

Selected bond distances (Å)	Selected bond angles (°)
-----------------------------	--------------------------

Re1-C3	1.918(6)	N1-Re1-N2	75.32(16)
Re1-C1	1.905(6)	C3-Re1-C2	87.7(2)
Re1-C2	1.919(6)	C1-Re1-N1	96.03(18)
Re1-N2	2.173(4)	C2-Re1-Br1	91.79(18)
Re1-N1	2.182(4)	C1-Re1-Br1	178.37(17)
Re1-Br1	2.629(10)	C3-Re1-Br1	89.90(16)
		N1-Re1-Br1	84.32(11)
		N2-Re1-Br1	83.98(12)

A dihedral angle of 14.2(2) °, between the equatorial plane (O2-C2-Re1-C3-O3) and the plane through the imidazo[4,5-*f*]1,10-phenanthroline ligand (N1, N2, C1-C12), is observed and expresses the significant bend of the (methoxyindole)imidazo[4,5-*f*]1,10-phenanthroline ligand out of the equatorial plane towards the bromido ligand (Figure S1).

The solid-state structure of **3a** is stabilised by one intramolecular weak interaction (C21-H21...N4), two intermolecular hydrogen bonding interactions (N3-H3A...O5, N5-H5A...Br1), three weak interactions (C11-H11...Br1, C24-H24...O4 and C25-H25C...O5), two Y-X...Cg π -interactions (Re1-Br1...Cg1 and S1-O5...Cg2) with X...Cg distances of 2.947(2) Å and 3.728(5) Å respectively, and an extensive network (forty nine) of π - π -interactions with Cg...Cg distances smaller than 3.8 Å (SI, Table S2-S3 and Figure S2). An infinite one-dimensional O-H...O-H chain along the *c*-axis is observed that is formed by the two hydrogen bonding interactions (N3-H3A...O5 and N5-H5A...Br1) (SI, Figure S3). The intra- and intermolecular interactions in the crystal structure of **3a** were quantified and confirmed using Hirshfeld surface analysis (SI, Figure S4 and S5). From the fingerprint plots of **3a**, it is clear that the H...H and O...H/H...O interactions contribute significantly to the packing and overall stabilisation of the crystal structure (SI, Figure S6).

Stability Studies of the Complexes

The stability of the complexes in phosphate buffer (pH 7.4) and FBS solution was monitored by UV/Vis absorption measurements over 6 hours. No isosbestic point was observed during the measurement of UV/Vis spectra of **1 - 8** in the buffer solution, however, a time-dependent decrease in absorbance was noticed (SI, Figure S7 - S10). This was due to the poor water solubility, which leads to precipitation of the complexes in aqueous solution. It is very important to note that the solubility of the complexes increases significantly in the presence of FBS, as recently observed with Ru(II) polypyridyl complexes (SI, Figure S11).⁵⁴ The stability of complexes **1 - 8** was also tested in DMSO solution (SI, Figure S7 - S10). Multiple isosbestic points were observed in the DMSO solution for complexes **6 - 8**, suggesting a binding with DMSO, which was not observed for complexes **1 - 5**. The binding of complexes **6** and **8** with DMSO was also confirmed by ESI-MS measurements (SI, Figure S12). In fact, observing the ESI-MS spectra for both complexes **6** and **8**, we noticed a DMSO-complex adduct ($[\text{Re}^{\text{I}}(\text{L6/8})(\text{CO})_3(\text{DMSO})]^+$) as well as a methanolic adduct ($[\text{Re}^{\text{I}}(\text{L6/8})(\text{CO})_3(\text{CH}_3\text{OH})]^+$). Moreover, a significant amount of the parent complex without the water ($[\text{Re}^{\text{I}}(\text{L6/8})(\text{CO})_3]^+$) was detected (SI, Figure S12). We suggest that the formation of the methanolic adduct is due to the presence of a high amount of methanol in the ESI-MS sample solution, replacing either the water molecule or the DMSO. Unfortunately, due to the poor solubility of complex **7** in methanol, we could not analyse the DMSO-binding using ESI-MS.

The stability of the complexes in DMSO was further confirmed by ¹H NMR; complexes **3** and **6** were dissolved in DMSO for 24 hours after which it was dried. The ¹H NMR spectrum of **3** was the same before and after 24 hours in DMSO (SI, Figure S13), confirming the results of the UV/Vis experiments. On the other hand, only 50% of **6** was still intact after it was dissolved in DMSO for

24 hours while 50% was the DMSO adduct. We confirmed that ~70% of the aqua complex **6** is still intact after it was dissolved in DMSO for 6 hours (SI, Figure S14).

Influence of H⁺ ions – Acid dissociation constant determination

Preliminary cytotoxicity studies indicated that **3** and **6** showed the best cytotoxicity and selectivity. For this reason, it was decided to proceed with **3** and **6** with a more detailed investigation, that also included intracellular accumulation, cellular uptake, mitochondrial respiration, cell death pathways and ROS generation.

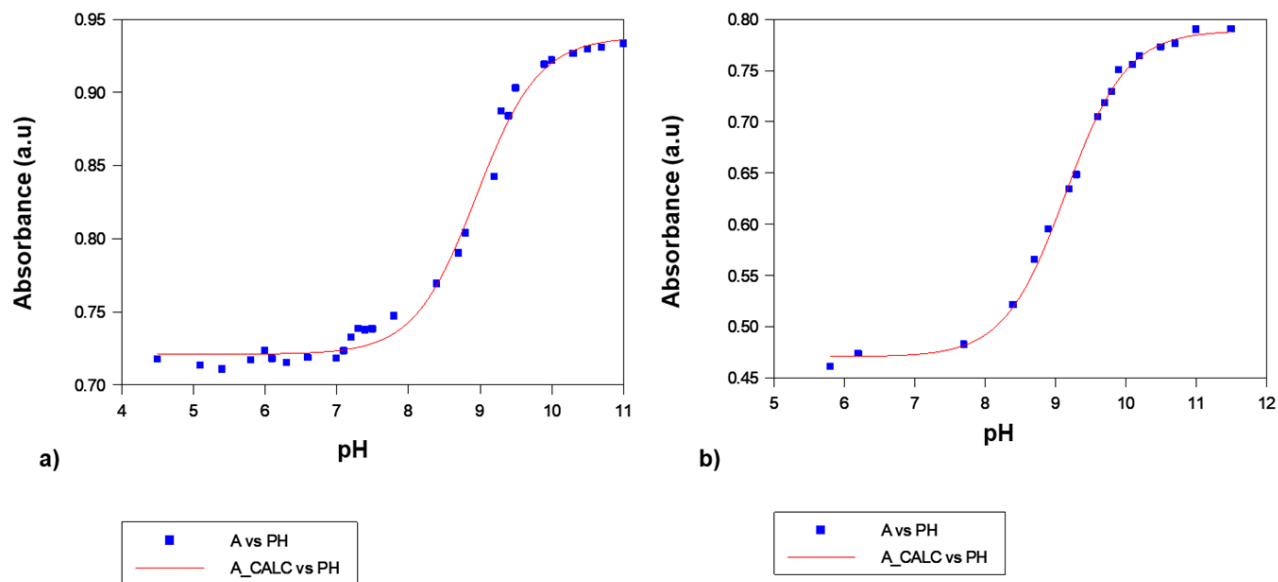
The pH dependence of **3** and **6** was studied at 25.0 °C from pH 5.5 to 11 in DMF:H₂O 7:3 (v/v %) solution. The stability of **3** and **6** in DMF:H₂O 7:3 (v/v %) at pH 5.5 for 24 hours was confirmed; the UV/Vis spectra is provided in the Supporting Information (Figures S15 and S16). Equation 1 describes the general acid/base behaviour of the monoprotic species HA, while equation 2 was utilised for the determination of the acid dissociation constants of **3** and **6**, where A is the absorbance at the specific pH, A_h the absorbance of the protonated species, A₀ the absorbance of the deprotonated species and K_a¹ is the acid dissociation constant.



$$A = \frac{A_h + A_0 \left(\frac{K_{a1}}{[\text{H}^+]} \right)}{1 + \left(\frac{K_{a1}}{[\text{H}^+]} \right)} \quad \text{Equation 2}$$

The acid dissociation constant of **3** and **6** were determined spectrophotometrically, by adjusting the pH of a 2×10^{-5} M solution of **3** and **6** at wavelengths 433 nm and 283 nm, respectively, whilst measuring the absorbance each time (SI, Figure S17 and S18). The non-linear fit of this data to equation 2 allowed for determining the pK_{a1} values of **3** and **6** as $8.95 (\pm 4)$ and $9.14 (\pm 2)$, respectively. This is illustrated in Figure 3. These values correspond with those of similar mononuclear deprotonation products and shows that the complexes are all in the aqua form under physiological conditions.^{55,56,57} Egli *et al.*⁵⁵ determined the pK_a values of $fac\text{-}[\text{Re}(\text{CO})_3(\text{H}_2\text{O})_3]^+$, yielding the deprotonation products $fac\text{-}[\text{Re}(\text{CO})_3(\text{H}_2\text{O})_2(\text{OH})]$ and $fac\text{-}[\text{Re}(\text{CO})_3(\text{H}_2\text{O})(\text{OH})_2]^-$, to be $pK_{a1} = 7.5 \pm 0.2$ and $pK_{a2} = 9.3 \pm 0.3$, respectively, while Schutte *et al.*⁵⁶ calculated the pK_a of $fac\text{-}[\text{Re}(\text{CO})_3(\text{Trop})(\text{H}_2\text{O})]$ (where Trop = tropolonato) to be 8.96 ± 0.02 . The pK_a of four rhenium dicarbonyl complexes ($[\text{Re}(\text{CO})_2(\text{N,N})(\text{P})(\text{H}_2\text{O})]^+$ with N,N = 1,10'-phenanthroline and 2,9-dimethyl 1,10-phenanthroline, P = PTA and DAPTA) were determined and were in the range 9.09 ± 0.03 to 9.28 ± 0.03 . Therefore, no considerable difference is observed in the pK_a values in these rhenium(I) complexes, whether the ligand *trans* to the aqua ligand is a carbonyl or phosphine ligand, or whether the bidentate ligand has N,N or O,O atom donors.

Figure 3. a) A plot of absorbance vs pH for **3**. $[\text{Re}] = 2 \times 10^{-5}$ M, 25 °C, 367 nm, $\mu = 1$ M (NaClO₄).
b) A plot of absorbance vs pH for **6**. $[\text{Re}] = 2 \times 10^{-5}$ M, 25 °C, 332 nm, $\mu = 1$ M (NaClO₄).



DNA binding study

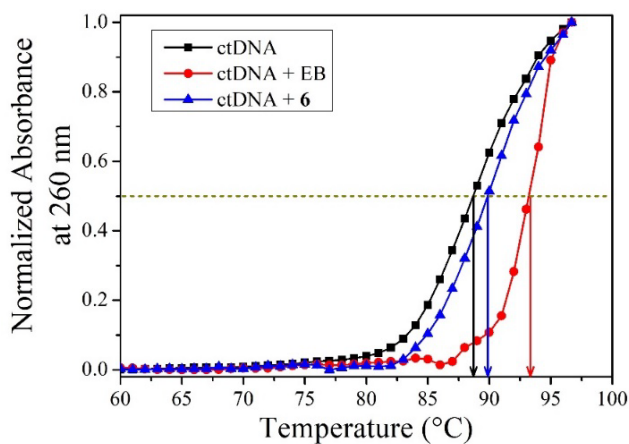
A preliminary UV/Vis DNA-complex titration study indicated that **6** has the highest binding constant in the series and, later on, we found out that **6** is the most cytotoxic complex in our hand. Hence, to check the possible ways of DNA binding by **6**, we have performed a) a binding study with a model nucleobase (guanosine) by ^1H NMR and ESI-MS for a possibility of covalent binding, b) ethidium bromide displacement assay for intercalation, and c) DNA melting assay to confirm the binding ability.

Surprisingly, in the ^1H NMR spectra of Guanosine binding kinetics, we only observed a secondary interaction of **6** with Guanosine, despite **6** having a labile neutral water molecule in the Re centre (SI, Figure S19 – S22). The binding study between the Re centre of complex **6** and N7

of Guanosine was monitored by ^1H NMR in DMF at 37°C (Figure S19 – S22). From the initial time (1 h), we observed a 0.015 ppm downfield shift of H_8 peak along with the shift of H_b and H_c . Considering H_a , we did not find any shift during the course of the study. This would suggest that the shift of the mentioned protons (H_b , H_c and H_8) is due to some secondary interaction but to the binding with N7 of guanosine with the Re centre. Moreover, the amine of guanosine is not taking part in the secondary noncovalent interaction (Figure S20). When we analysed the same solution by ESI-MS, we found a little peak of **6** and a guanosine adduct along with an important amount of free ligand (SI, Figure S23). However, we could not find any alteration of ^1H NMR peaks of **6** with time (SI, Figure S19) and the peaks were not shifted in the ^1H NMR spectra studying the stability of **6** (SI, Figure S23). Hence, the formation of the adduct and the degradation of **6** have occurred only in the ESI-MS measurement conditions. Therefore, we deduced that the complex cannot form any covalent bond with DNA *via* the Re centre.

The presence of a planar ring system increases the possibility of DNA intercalation. Hence, to measure the intercalation ability of **6**, we performed an ethidium bromide (EB) displacement assay by fluorescence quenching of EB-DNA adduct (SI, Figure S24). The apparent binding constant for intercalation of **6** with ctDNA is in the order of $3.9 (1) \times 10^6 \text{ M}^{-1}$, suggesting the possible targeting of DNA via intercalation. Finally, the DNA binding properties of complex **6** was confirmed by measuring DNA melting temperature (Figure 4). We observed a shift of ctDNA melting temperature towards higher temperature of **6** bound ctDNA (ΔT_m ; $1 \pm 0.4^\circ\text{C}$ and $4 \pm 0.1^\circ\text{C}$ for **6** and EB respectively, (Figure 4) in comparison to unbound/normal ctDNA melting temperature.

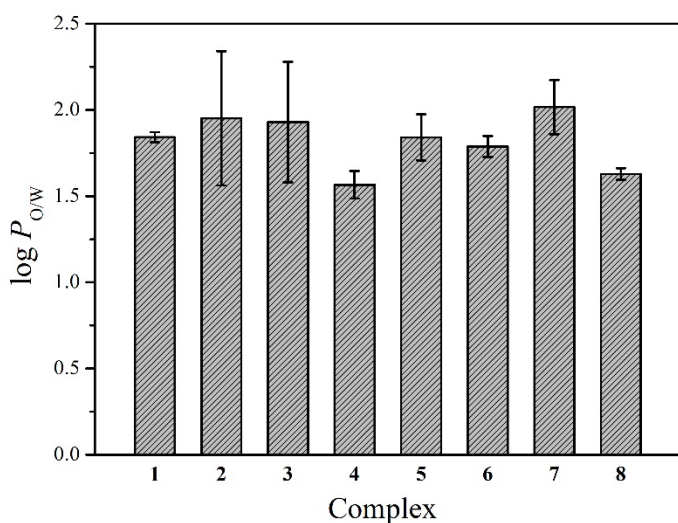
Figure 4. ctDNA melting curve. Conc. of ctDNA was $40 \mu\text{M}$, conc. of EB and **6** was $30 \mu\text{M}$. from temp $60\text{-}97^\circ\text{C}$, holding time 1 min, $1^\circ\text{C}/\text{min}$ and recorded abs each 1°C change in temp.



Distribution coefficient (logP values)

The distribution coefficient (logP value) of the complexes was determined using the standard Shake-Flask method.⁵⁸ All the complexes showed almost equal distribution coefficients within 1.5 - 2.0 (Figure 5), suggesting hydrophobicity. This suggests that the derivatization on the N-N bidentate ligand of Re complexes might not be very useful to change the solubility and lipophilicity of the compounds. Overall, the logP values of our complexes compared well with other Re tricarbonyl compounds reported in the literature.^{30,59}

Figure 5. The above bar plot represents the logP values of complexes **1 - 8**.



BSA binding

Serum albumin is the most abundant protein present in the blood and plays an important role in the delivery of hydrophobic compounds to the cell. Importantly, serum albumin contains a free thiol from 34-cysteine^{60,61,62,63} and Re complexes have very high binding affinity for sulphur donors.^{64,65} BSA has an intrinsic fluorescence emission maximum at 341 nm upon excitation at 280 nm.^{66,67} The internal fluorescence quenching was observed upon binding with our compound. Hence, fluorescence titrations between BSA and different concentrations of the complex were performed to measure the binding constant. The bovine serum albumin (BSA) binding study suggests that all complexes can bind BSA with moderately high binding constant in the order of 10^5 M^{-1} except complex 7 (Table 2, Figures S25 – S28). A significantly low binding constant was observed for 7 ($0.4 \times 10^5 \text{ M}^{-1}$). The Stern-Volmer quenching constant signifies the distance between an inhibitor and the fluorescence-originating molecules.^{68,69,70} The decrease of Ksv indicates a long distance between the inhibitor and fluorescence protein. We observed the Ksv in the order of 10^4 M^{-1} , suggesting a moderate fitting in the hydrophobic pocket of BSA.

Table 2. The affinity of complexes 1 - 8 for BSA.

Complex	Stern-Volmer quenching constant ($K_{sv} \times 10^4, M^{-1}$)	Binding constant ($K_a \times 10^5, M^{-1}$)	Number of binding sites (n)
1	2.41 ± 0.05	2.71 ± 2.91	1.23 ± 0.13
2	1.06 ± 0.03	1.10 ± 0.79	1.24 ± 0.08
3	2.98 ± 0.15	1.81 ± 1.16	1.18 ± 0.07
4	2.95 ± 0.09	1.46 ± 0.06	1.18 ± 0.01
5	2.57 ± 0.07	1.04 ± 0.30	1.15 ± 0.03
6	2.82 ± 0.07	2.29 ± 0.98	1.23 ± 0.05
7	0.83 ± 0.03	0.40 ± 1.16	1.16 ± 0.03
8	1.60 ± 0.10	0.94 ± 1.11	1.10 ± 0.20

All plots are available in the supplementary file, SI, Figure S25 – S28.

Cytotoxicity

The *in vitro* anticancer activity of the complexes was determined against human prostate cancer (PC3) and compared with the normal retinal pigment epithelial-1 (RPE-1) cells. The results are summarized in Table 3. Among the eight complexes, **4** - **6** showed cytotoxicity in the low nanomolar range (0.04, 0.03 and 0.05 μ M, respectively). Such low values are scarce in the literature for similar compounds. However, the three complexes are highly cytotoxic against normal RPE-1 cells as well (0.12, 0.27 μ M and 0.65 μ M, respectively). Despite this, it is very exciting to notice that almost all complexes are more toxic against cancer cells than normal cells. Complex **3** is the most promising by showing a 26-fold selectivity with an IC_{50} value of 0.32 μ M against PC3 cells. Additionally, it is almost 21 times more cytotoxic than cisplatin against PC3 cells. Interestingly, it was observed by ICP-MS that the most selective complexes **3** and **6** were localizing in mitochondria and nuclei, respectively, suggesting that they have a different mode of action. In general, we observed that a fused ring or similar derivatization in the N-N bidentate ligand could be useful to increase cytotoxicity. Very interestingly, comparing complexes **2** and **3**, the introduction of a methoxy moiety in the indole ring of **2** showed a positive impact on the IC_{50} values with an increase of almost 15-fold in cytotoxicity.

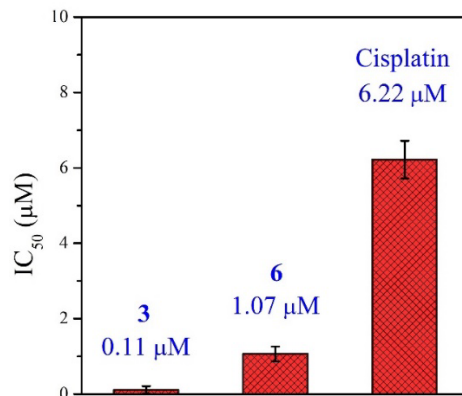
Table 3. Cytotoxicity of complexes **1 - 8** under the normoxic conditions in comparison to cisplatin.

Complex	IC ₅₀ (μM) ± S.D. ^a		Selectivity ^b
	PC3	RPE-1	
1	4.6 ± 0.5	0.36 ± 0.02	-
2	5 ± 3	23 ± 2	5
3	0.32 ± 0.03	8.2 ± 0.4	26
4	0.04 ± 0.01	0.12 ± 0.01	3
5	0.03 ± 0.01	0.27 ± 0.02	9
6	0.05 ± 0.01	0.65 ± 0.03	13
7	1.4 ± 0.40	4.2 ± 0.5	3
8	0.41 ± 0.04	1.79 ± 0.04	4
Cisplatin	6.9 ± 0.5	36 ± 4	5

^aS.D. is the standard deviation. The IC₅₀ value was determined using the standard Resazurin assay after 48 h of treatment under normoxic conditions (~ 15 % O₂ level). The representative plots are provided in SI, Figures S29 – S33. ^bSelectivity represents the ratio between IC₅₀ against RPE-1 and IC₅₀ against PC3 cells.

Despite the high cytotoxic activity of complexes against PC3 cells in normoxia, a decrease in cytotoxicity (IC₅₀, μM: 5.5 ± 1.3 for **3** and 7.0 ± 2.2 for **6**) was observed for complexes **3** and **6** when they were evaluated in hypoxic conditions (SI, Table S4). However, a decrease in cytotoxicity of cisplatin (IC₅₀, μM: >50) in hypoxic conditions was also observed. Hence, in hypoxic conditions, despite the decreased cytotoxicity of **3** and **6** against PC3 cells, they were still around 10 times more active than cisplatin. Very importantly, when the compounds were tested against 3D multicellular PC3 cell spheroids, we observed a small decrease in IC₅₀ concentration (Figure 6), indicating that the compounds are efficient in penetrating the more tumor-like environment of cell spheroids.

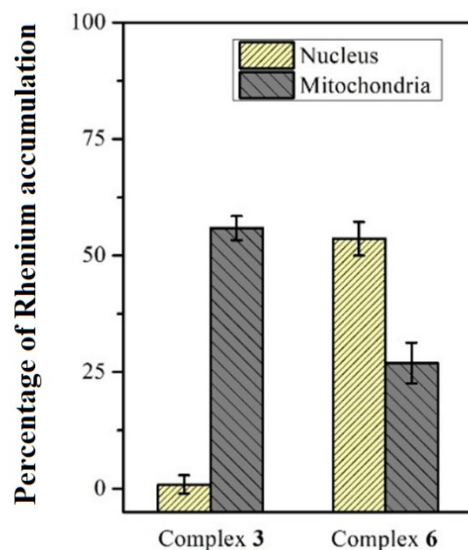
Figure 6. The IC₅₀ values represent the cytotoxicity of complexes against 3D multicellular PC3 cells spheroid (average diameter 435 μm) after 72 hours of incubation with the respective complexes in normoxic conditions, determined using AlamarBlue assay.



Intracellular accumulation study

Most of the rhenium(I) carbonyl complexes reported so far preferentially target mitochondria.^{14,32,59,71} In order to investigate the possible cellular target of the complexes, we measured the accumulation of complexes **3** and **6** in the nuclei and mitochondria using cell fractionation and ICP-MS, and not using the intrinsic luminescent properties of the Re(I) tricarbonyl complex. In fact, it was reported that different cellular accumulations results were observed between these methods since the luminescence properties of this type of metal complexes are environment-dependent and can alter the confocal results.^{72,73,74} We found that **3** targets the mitochondria, whereas **6** mostly targets the nuclei and, to a lesser extent, the mitochondria (Figure 7). This observation is interesting since there are very few examples of Re(I) tricarbonyl complexes that target the nuclei.

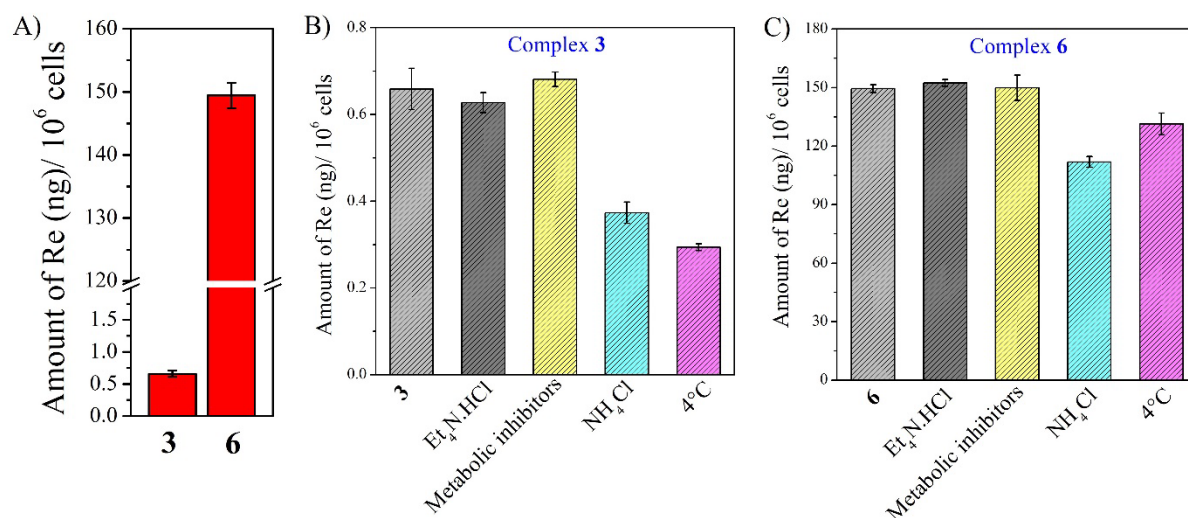
Figure 7. Percentage of Re(I) accumulation in the nucleus and mitochondria compared to total uptake by PC3 cells. The amount of rhenium in the isolated nucleus and mitochondria from complex-treated PC3 cells was quantified using ICP-MS.



Cellular uptake and uptake pathways

The cellular uptake pathways of complexes **3** and **6** have been investigated using known uptake pathways inhibitors viz., 1 mM tetraethylammonium chloride (cationic transporter inhibitor),⁷⁵ 5 μ M oligomycin and 50 mM 2-Deoxy-D-glucose (metabolic inhibitors),^{76,77} and 50 mM ammonium chloride (endocytotic inhibitor).^{78,79,80} The cells were pre-treated with the respective inhibitors to block the transporter channel. Hence, the uptake of complex might get affected if the complex utilizes those transporters. For both complexes **3** and **6**, a significantly less amount of complex uptake was observed in the presence of an endocytotic inhibitor (i.e., ammonium chloride)^{78,79,80} and at 4°C in comparison to the control (Figure 8B and 8C). Hence, the result suggests that endocytotic and passive diffusions were majorly involved in complex uptake. Surprisingly, a significantly high uptake of complex **6** was observed compared to **3**, which could explain the low nanomolar cytotoxicity of **6** (Figure 8A).

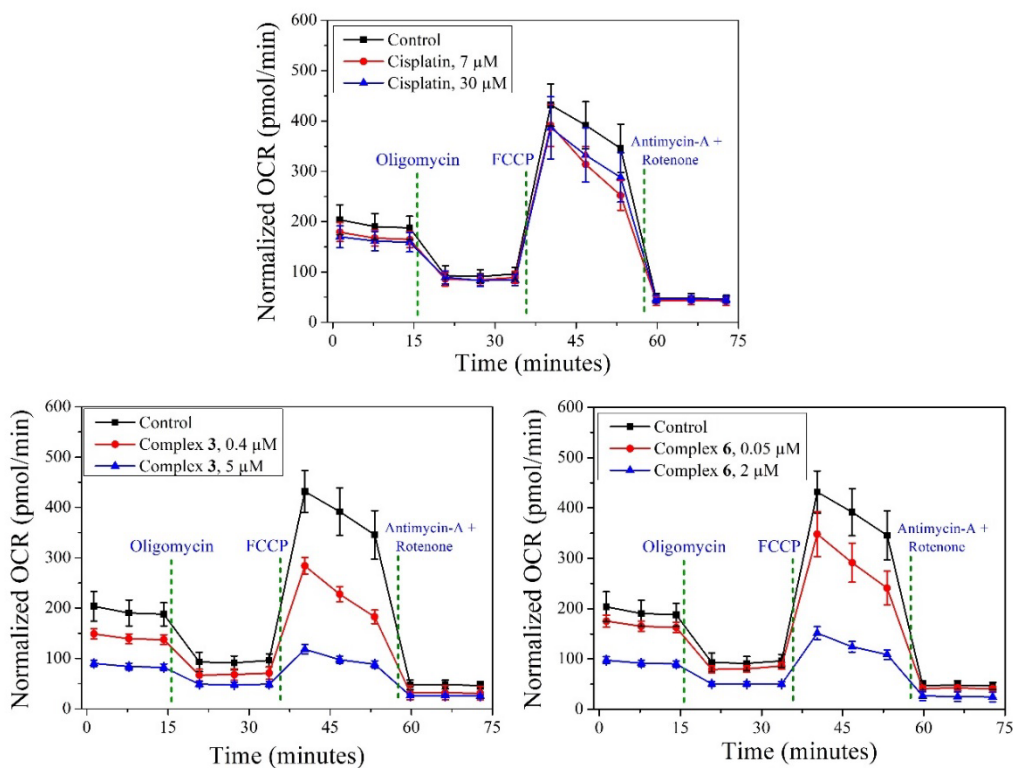
Figure 8. The figure represents the ng of rhenium in PC3 cells upon 2 hours of incubation with either complex **3** or **6**, in the presence and absence of cellular uptake pathways inhibitor. The amount of Re was quantified by ICP-MS. 1 mM tetraethylammonium chloride (cationic transporter inhibitor), 5 μ M oligomycin and 50 mM 2-Deoxy-D-glucose (metabolic inhibitors), and 50 mM ammonium chloride (endocytotic inhibitor) were used.



Mitochondrial Respiration test

Since a significant amount of the complexes **3** and **6** accumulated in mitochondria, the possible influence of the compounds in the PC3 cells' oxygen consumption was measured by the Mito stress test using a Seahorse XF Analyzer. In both cases, a significant amount of concentration-dependent mitochondrial dysfunction was identified. Initially, a concentration-dependent lowering of basal respiration was observed for both complexes **3** and **6** (Figure 9 and SI, Figure S34). Furthermore, a significant drop in ATP production was identified (SI, Figure S35).

Figure 9. Mito stress test profile in PC3 cells measured by Seahorse Xef4 after 24 h treatment with complexes **3**, **6** and cisplatin in normoxic condition. OCR stands for oxygen consumption rate. The experiment was performed using specific electron transport chain inhibitors, viz., Oligomycin (inhibitor of ATP synthase (complex V)), FCCCP (uncoupling agent), antimycin-A (complex III inhibitors), and rotenone (complex I inhibitor).



Cell death pathways and ROS generation

The cell death pathways induced by **3** and **6** in PC3 cells were analysed by measuring cytotoxicity in the presence of specific cell death pathway inhibitors viz., 3-Methyladenine (autophagy), Z-VAD-FMK (apoptosis), cycloheximide (paraptosis) and necrostatin-1 (necrosis). A significant amount of increase in the IC₅₀ value (around 2 times) of complex **3** against paraptosis inhibitor-treated PC3 cells was observed (Figure 10). Finally, the paraptosis induction in PC3 cells by complex **3** was confirmed by observing vacuole formations in the bright field image of PC3 cells treated with compound **3** (SI, Figure S36). Of note, similar kinds of Re complexes are known to

induce cell death by paraptosis.^{38,59} In the case of complex **6**, a very little decrease in IC₅₀ dose was noticed when the cells were pre-treated with an apoptosis inhibitor (Figure 10). Hence, we performed the well-known annexin-V assay to confirm the apoptosis pathway. As we found a non-apoptosis pathway for cell killing during IC₅₀ dose determination of **3** in the presence of an apoptosis inhibitor (Figure 10), complex **3** did not induce apoptosis whereas for complex **6**, a concentration-dependent induction of apoptosis was observed (Figure 11). However, the amount of apoptosis induction by **6** was very low (Figure 11), suggesting that apoptosis may not be a major pathway for cell killing. In the case of cisplatin, we observed an important increase of the IC₅₀ value in the presence of both apoptosis and autophagy inhibitors (Figure 10). The observed apoptosis and autophagy induction by cisplatin agrees with literature reports.⁸¹

Figure 10. The above figure represents the IC₅₀ values of respective complexes against PC3 cells in the presence of inhibitors in comparison to the cytotoxicity without any inhibitor. The inhibitors were pre-incubated for 1 hour. The respective metal complexes were then loaded and incubated for 36 hours in normoxic conditions (details in experimental section).

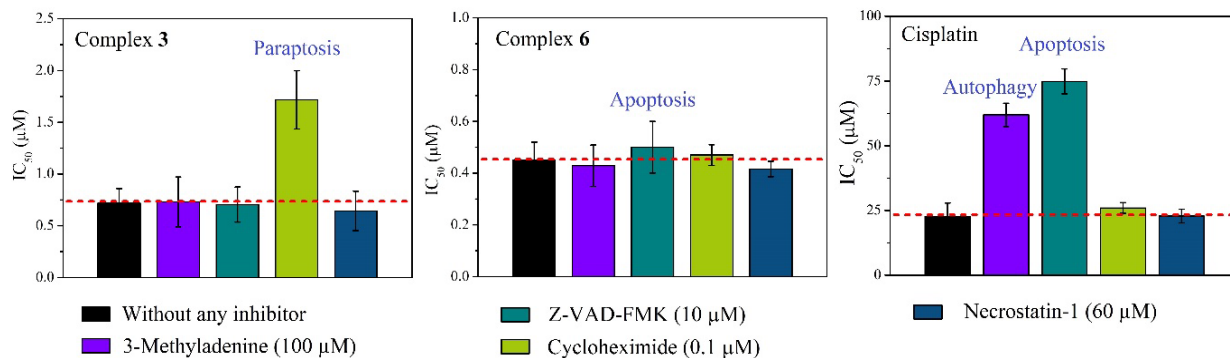
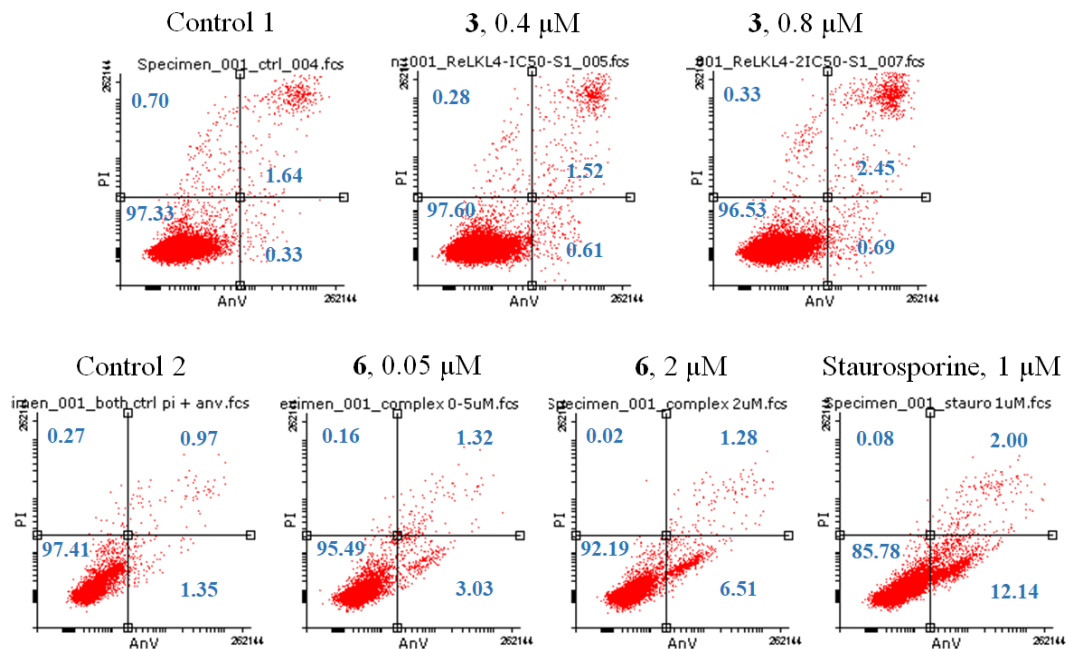


Figure 11. Induction of apoptosis of compound treated PC3 cells were measured by flow cytometry after 24 h compound exposure. The compound treated cells were stained dually with Annexin V-PE and PI prior to analysis. Lower left quadrant (both Annexine V and PI negative fraction): intact cells. Lower right quadrant (Annexine V positive/ PI negative fraction): early

apoptosis. Upper right quadrant (Annexine V positive/ PI positive fraction): late apoptosis, and upper left quadrant (Annexine V negative/ PI positive fraction): necrosis. Staurosporine, an apoptosis inducer, was used as positive control.



Metal complexes are very well known to generate ROS due to the presence of easily accessible multiple oxidation states. The generation of ROS inside the PC3 cells treated with the two Re derivatives was analysed using a standard ROS detection kit. The result suggested that the compounds do not play a role in altering the ROS homeostasis of the cells. In fact, after treatment with complexes **3** and **6**, the ROS level (SI, Figure S37) inside the cells was similar to the control.

Conclusion

This study reports the synthesis, characterisation, DNA binding mode and *in vitro* cytotoxicity of eight rhenium(I) tricarbonyl complexes. All complexes showed stability in aqueous solution and can bind to BSA with binding constants ranging from 10^4 to 10^5 M⁻¹. The pKa values of **3** and

6 indicate that these complexes will be in the aqua form under biological conditions. The Re(I) carbonyl complexes showed exceptionally low nanomolar cytotoxicity against prostate adenocarcinoma (PC3) and a degree of selectivity towards cancer cells over normal human retinal pigment epithelial-1 (RPE-1) cells. The most selective complexes **3** and **6** were found to localise in mitochondria and nuclei, respectively. Moreover, both complexes **3** and **6** downregulated the mitochondrial ATP production in PC3 cells. The most selective complex **3** followed a paraptosis pathway for cell killing. On the other hand, despite the intercalation of complex **6** with DNA, and the induction of mitochondrial dysfunction after treatment, only a very little percentage of cells induced apoptosis. This suggests that apoptosis is a minor pathway for cell killing. Surprisingly, **6** did not follow any of the other tested cell death pathways, i.e. necrosis, autophagy or paraptosis. Very interestingly, this suggests that the presence of different functional groups on the same phenanthroline ligand core could induce different cell death mechanisms, still maintaining an IC₅₀ range very promising.

Experimental Section

General procedures and instrumentation

The IR spectra were recorded at room temperature on a PerkinElmer BX II IR spectrometer in the range 4000 – 370 cm. The liquid-state ¹H and ¹³C{¹H} NMR spectra were recorded at 25.0 °C on a 600 MHz Avance II Bruker spectrometer operating at 600 MHz and 151 MHz for ¹H and ¹³C respectively, and dimethyl sulfoxide-d₆ (DMSO-d₆) was used as solvent. The chemical shifts (δ) are reported in parts per million (ppm); for DMSO-d₆, the spectra were referenced relative to the solvent peak (2.50 ppm for ¹H and 39.52 ppm for ¹³C). Coupling constants (*J*) are reported in Hz. Electrospray ionization Mass Spectrometry (ESI-MS) of **1** - **8** were recorded on a SCIEX 4000 QTRAP hybrid triple quadrupole ion trap mass spectrometer either in positive or in negative ESI

mode with samples injected as methanol solutions. The ionisation voltage was set at 5500 V in positive mode with a 10 psi curtain gas setting and 20 psi ionisation gas (GS1) setting. The UV/Vis spectra were recorded in the range of 100 – 1100 nm at room temperature on a LAMBDA 265 UV/Visible Spectrophotometer. The spectrometer utilises a Xenon Flash interface. The intensity data was collected on a Bruker X8 ApexII 4K Kappa CCD diffractometer, equipped with graphite monochromated Mo K(α) radiation with a wavelength of 0.71073 Å, using an exposure time of 20 seconds/frame. A total of 1568 frames was collected with a frame width of 0.5° with 99.7% completeness accomplished. Phi and omega-scans are reported at 100 K. All cell refinements as well as data reductions were performed using SAINT-Plus software.⁸² Absorption corrections were made using the multi-scan technique and the SADABS software package. All structures were solved with the SIR-97 software package,⁸³ and structure refinement was made using SHELXL-2013⁸⁴ and WinGX.⁸⁵ The molecular graphics were drawn using DIAMOND.⁸⁶ All non-hydrogen atoms were refined anisotropically. Methyl and aromatic hydrogen atoms were placed in geometrically idealized positions and constrained to ride on their parent atoms, with C–H = 0.98 and 0.95 Å and $U_{\text{iso}}(\text{H}) = 1.5U_{\text{eq}}(\text{C})$ and $1.2U_{\text{eq}}(\text{C})$ respectively. The NH hydrogen atoms were located in the difference-Fourier map and freely refined with $U_{\text{iso}}(\text{H}) = 1.5U_{\text{eq}}(\text{N})$. The Fc versus Fo plot proved five reflections to be outliers, and they were removed from the refinement as systematic errors.

Synthesis

The starting synthon *fac*-[NEt₄]₂[Re(CO)₃(Br)₃] (ReAA) and the ligands 2,6-dimethoxypyridyl)imidazo[4,5-*f*]1,10-phenanthroline (**L1**), (indole)imidazo[4,5-*f*]1,10-phenanthroline (**L2**), (5-methoxyindole)imidazo[4,5-*f*]1,10-phenanthroline (**L3**), (biphenyl)-imidazo[4,5-*f*]1,10-phenanthroline (**L4**), (fluorene)imidazo[4,5-*f*]1,10-phenanthroline (**L5**),

(benzo[b]thiophene)imidazo[4,5-*f*]1,10-phenanthroline (**L6**), (5-bromothiazole)imidazo[4,5-*f*]1,10-phenanthroline (**L7**), and (4,5-dimethylthiophene)imidazo[4,5-*f*]1,10-phenanthroline (**L8**) has been synthesized and characterised as reported previously in literature.^{45,87} $^{13}\text{C}\{^1\text{H}\}$ NMR was attempted for **1** – **8**, however, after 18 000 scans on highly concentrated NMR samples, poor or no peaks were obtained. Due to economic implications, other characterisation methods were relied upon.

General synthetic procedure for Re(I) tri carbonyl complexes.

ReAA was added to 3 eq. of AgNO_3 solution in 10 mL water (at pH 2) and stirred at room temperature for 24 hours, which resulted in a grey/white precipitate of AgBr. The precipitate was filtered off and 1.1 equivalent of the ligand was added to the filtrate. The solution was stirred at 80 °C for 12 hours and a solid separated from the solution. The reaction mixture was filtered and washed three times with distilled water to yield a solid product.

fac-[Re(CO)₃(L1)(H₂O)][NO₃] (**1**)

0.206 g (0.267 mmol) ReAA, 0.136 g (0.801 mmol) AgNO_3 , 0.099 g (0.294 mmol) **L1**. Yield: 0.0902 g (0.131 mmol, 49%); Elemental analysis for $\text{C}_{23}\text{H}_{17}\text{N}_6\text{O}_9\text{Re}$: Calculated: C = 39.04%, N = 11.88%, H = 2.42%; Found: C = 38.91%, N = 11.90%, H = 2.44%.; IR (ATR, cm^{-1}): $\nu_{\text{N-H}} = 3346$, $\nu_{\text{O-H}} = 3064$, 2958, $\nu_{\text{C=O}} = 2028$, 1896, $\nu_{\text{C=N}} = 1605$, $\nu_{\text{C=N}} = 1582$, 1452, $\nu_{\text{C-O}} = 1323$, 1274.; ^1H NMR (400 MHz, DMSO-*d*₆): δ 9.5 (4H, m), 8.6 (1H, d, $J = 8.2$ Hz), 8.2 (2H, bs), 6.7 (1H, d, $J = 8.2$ Hz), 4.2 (3H, s), 4.0 (3H, s) ppm; $^{13}\text{C}\{^1\text{H}\}$ NMR (151 MHz, DMSO-*d*₆): δ 196.9, 164.2, 163.9, 159.8, 159.6, 150.0, 142.5, 142.3, 124.6, 105.1, 104.6, 103.2, 102.9, 54.6, 54.5, 54.4, 54.3 ppm. UV/Vis (DMSO): $\lambda_{\text{max}} = 350$ nm, $\epsilon = 12\,223$ M⁻¹ cm⁻¹. ESI-MS (CH₃OH, +ve ion mode): m/z 627.9 ([M - NO₃⁻ - H₂O]⁺); calcd, 627.6).

fac-[Re(CO)₃(L2)(H₂O)][NO₃] (**2**)

0.201 g (0.260 mmol) ReAA, 0.132 g (0.777 mmol) AgNO₃, 0.096 g (0.286 mmol) **L2**. Yield: 0.098 g (0.143 mmol, 55%); Elemental analysis for C₂₄H₁₅N₆O₇Re: Calculated: C = 42.04%, N = 12.26%, H = 2.21%; Found: C = 41.94%, N = 12.31%, H = 2.19%; IR (ATR, cm⁻¹): ν_{N-H} = 3387, ν_{O-H} = 3074, ν_{C=O} = 2019, 1912, 1886, ν_{C=N} = 1576, ν_{C=N} = 1318; ¹H NMR (400 MHz, DMSO-d₆): δ 9.4 (4H, overlying multiplet, singlet and doublet), 8.7 (1H, s), 8.3 (2H, overlying singlets), 8.1 (1H, s), 7.6 (1H, s), 7.3 (2H, s) ppm; ¹³C{¹H} NMR (151 MHz, DMSO-d₆): δ 197.0, 143.6, 137.0, 134.3, 127.2, 127.1, 125.5, 123.1, 121.8, 121.1, 112.7 ppm; UV/Vis (DMSO): λ_{max} = 345 nm, ε = 23 989 M⁻¹ cm⁻¹. ESI-MS (CH₃OH, +ve ion mode): m/z 606.2 ([M - NO₃⁻ - H₂O]⁺); calcd, 605.6).

***fac*-[Re(CO)₃(L3)(H₂O)][NO₃] (3)**

0.20 g (0.260 mmol) ReAA, 0.132 g (0.780 mmol) AgNO₃, 0.104 g (0.286 mmol) **L3**. Yield: 0.0614 g (0.0858 mmol, 33%); Elemental analysis for C₂₅H₁₇N₆O₈Re: Calculated: C = 41.96%, N = 11.74%, H = 2.39%; Found: C = 41.86%, N = 11.72%, H = 2.38%; IR (ATR, cm⁻¹): ν_{N-H} = 3121, ν_{O-H} = 2921, 2852, ν_{C=O} = 2028, 1936, 1910, ν_{C=N} = 1603, ν_{C=N} = 1319, ν_{C-O} = 1217. ¹H NMR (600 MHz, DMSO-d₆): δ 11.7 (1H, s), 9.3 (2H, broad singlet), 9.2 (2H, singlet), 8.2 (2H, broad singlet), 8.1 (2H, s), 7.5 (1H, d, *J* = 8.7 Hz), 6.9 (1H, d, *J* = 8.6 Hz), 3.9 (3H, s) ppm. ¹³C{¹H} NMR (151 MHz, DMSO-d₆): δ 155.1, 132.1, 126.1, 125.7, 113.3, 113.0, 103.6, 55.9 ppm. UV/Vis (DMSO): λ_{max} = 390 nm, ε = 19 145 M⁻¹ cm⁻¹; ESI-MS (CH₃OH, +ve ion mode): m/z 636.2 ([M - NO₃⁻ - H₂O]⁺); calcd, 635.6).

***fac*-[Re(CO)₃(L4)(H₂O)][NO₃] (4)**

0.102 g (0.132 mmol) ReAA, 0.067 g (0.397 mmol) AgNO₃, 0.054 g (0.145 mmol) **L4**. Yield: 0.0219 g (0.0303 mmol, 23%). Elemental analysis for C₂₈H₁₈N₅O₇Re: Calculated: C = 46.53%, N = 9.69%, H = 2.51%; Found: C = 46.23%, N = 9.71%, H = 2.48%. IR (ATR, cm⁻¹): ν_{O-H} = 3091, 3027, ν_{C=O} = 2038, 1993, 1956, ν_{C=C} = 1808, 1775, 1610, ν_{C=N} = 1554, ν_{C=N} = 1339. ¹H NMR (600

MHz, DMSO-d₆): δ 13.9 (1H, s), 9.1 (4H, s), 8.3 (2H, d, $J = 7.3$ Hz), 8.0 (2H, broad singlet), 7.9 (2H, d, $J = 7.4$ Hz), 7.8 (2H, d, $J = 7.0$ Hz), 7.5 (2H, t, $J = 13.8, 6.9$ Hz), 7.4 (1H, t, $J = 13.8, 6.9$ Hz) ppm. $^{13}\text{C}\{^1\text{H}\}$ NMR (151 MHz, DMSO-d₆): δ 151.6, 141.9, 139.6, 129.5, 129.0, 128.5, 127.7, 127.4, 127.2, 125.1 ppm. UV/Vis (DMSO): $\lambda_{\text{max}} = 337$ nm, $\epsilon = 25\,793\text{ M}^{-1}\text{ cm}^{-1}$. ESI-MS (CH₃OH, +ve ion mode): m/z 643.2 ($[\text{M} - \text{NO}_3^- - \text{H}_2\text{O}]^+$); calcd, 642.6).

***fac*-[Re(CO)₃(L5)(H₂O)][NO₃] (5)**

0.10 g (0.130 mmol) ReAA, 0.066 g (0.39 mmol) AgNO₃, 0.055 g (0.143 mmol) L5. Yield: 0.0343 g (0.0469 mmol, 36%). Elemental analysis for C₂₉H₁₈N₅O₇Re: Calculated: C = 47.41%, N = 9.53%, H = 2.47%; Found: C = 47.44%, N = 9.50%, H = 2.43%. IR (ATR, cm⁻¹): $\nu_{\text{N-H}} = 3471$, $\nu_{\text{O-H}} = 3057, 2902$, $\nu_{\text{C=O}} = 2028, 1926, 1905$, $\nu_{\text{C=N}} = 1610$, $\nu_{\text{C=C}} = 1557, 1476$, $\nu_{\text{C-H}} = 1446$, $\nu_{\text{C=N}} = 1317$. ^1H NMR (600 MHz, DMSO-d₆): δ 9.1 (4H, merged singlet), 8.3 (1H, s), 8.2 (1H, d, $J = 7.6$ Hz), 8.0 (3H, merged singlet), 7.9 (1H, d, $J = 4.6$ Hz), 7.6 (1H, d, $J = 7.3$ Hz), 7.3 (2H, dt, $J = 29.2, 7.3$ Hz), 4.0 (2H, s) ppm. $^{13}\text{C}\{^1\text{H}\}$ NMR (151 MHz, DMSO-d₆): δ 152.2, 146.7, 144.1, 144.0, 143.1, 140.7, 139.2, 128.2, 127.8, 127.4, 125.7, 125.6, 125.1, 123.2, 120.9, 120.8, 36.8 ppm. UV/Vis (DMSO): $\lambda_{\text{max}} = 342$ nm, $\epsilon = 29\,853\text{ M}^{-1}\text{ cm}^{-1}$. ESI-MS (CH₃OH, +ve ion mode): m/z 655.2 ($[\text{M} - \text{NO}_3^- - \text{H}_2\text{O}]^+$); calcd, 654.7).

***fac*-[Re(CO)₃(L6)(H₂O)][NO₃] (6)**

0.199 g (0.258 mmol) ReAA, 0.131 g (0.774 mmol) AgNO₃, 0.10 g (0.283 mmol) L6. Yield: 0.105 g (0.149 mmol, 58%). Elemental analysis for C₂₄H₁₄N₅O₇SRe: Calculated: C = 41.02%, N = 9.97%, S = 4.56%, H = 2.01%; Found: C = 41.20%, N = 9.96%, S = 4.60%, H = 2.02%. IR (ATR, cm⁻¹): $\nu_{\text{N-H}} = 3397$, $\nu_{\text{O-H}} = 3075$, $\nu_{\text{C=O}} = 2028, 1920, 1894$, $\nu_{\text{C=N}} = 1660$, $\nu_{\text{C=C}} = 1581, 1562$, $\nu_{\text{C=N}} = 1370, 1304$. ^1H NMR (400 MHz, DMSO-d₆): δ 9.5 (1H, dd, $J = 15.3, 4.7$ Hz), 9.3 (1H, broad singlet), 9.1 (2H, overlapping singlets), 8.3 (2H, overlapping singlets), 8.0 (3H, m), 7.5 (2H,

overlapping signals) ppm. $^{13}\text{C}\{^1\text{H}\}$ NMR (101 MHz, DMSO- d_6): δ 196.9, 152.8, 148.6, 140.2, 140.0, 139.9, 133.2, 132.8, 127.6, 126.6, 126.2, 125.7, 125.5, 125.3, 125.2, 124.9, 124.2, 123.4, 123.2, 123.0 ppm. UV/Vis (DMSO): $\lambda_{\text{max}} = 369$ nm, $\epsilon = 28\,040$ $\text{M}^{-1} \text{cm}^{-1}$. ESI-MS (CH_3OH , +ve ion mode): m/z 623.1 ($[\text{M} - \text{NO}_3^- - \text{H}_2\text{O}]^+$); calcd, 622.6).

***fac*-[Re(CO)₃(L7)(H₂O)][NO₃] (7)**

0.206 g (0.267 mmol) ReAA, 0.136 g (0.801 mmol) AgNO₃, 0.112 g (0.294 mmol) L7. Yield: 0.0254 g (0.0347 mmol, 13%). Elemental analysis for C₁₉H₁₀N₆O₇SBrRe: Calculated: C = 31.15%, N = 11.47%, S = 4.37%, Br = 10.91%, H = 1.37%; Found: C = 31.25%, N = 11.51%, S = 4.41%, Br = 10.89%, H = 1.35%. IR (ATR, cm^{-1}): $\nu_{\text{N-H}} = 3398$, $\nu_{\text{O-H}} = 3059$, $\nu_{\text{C=O}} = 2025$, 1918, 1893, $\nu_{\text{C=N}} = 1608$, $\nu_{\text{C=N}} = 1312$, 1254, $\nu_{\text{C-Br}} = 805$, $\nu_{\text{C-S}} = 805$. ^1H NMR (400 MHz, DMSO- d_6): δ 13.9 (1H, s), 11.7 (1H, s), 9.5 (2H, s), 8.2 (3H, overlying singlets), 7.5 (1H, triplet, $J = 16.9, 8.72$), 6.9 (1H, doublet, $J = 8.7$ Hz) ppm. $^{13}\text{C}\{^1\text{H}\}$ NMR (101 MHz, DMSO- d_6): δ 197.0, 159.0, 152.4, 145.3, 140.0, 128.1, 124.5 ppm. UV/Vis (DMSO): $\lambda_{\text{max}} = 261$ nm, $\epsilon = 1\,494$ $\text{M}^{-1} \text{cm}^{-1}$. ESI-MS (CH_3OH , +ve ion mode): m/z 671.1 ($[\text{M} - \text{NO}_3^-]^+$); calcd, 670.5).

***fac*-[Re(CO)₃(L8)(H₂O)][NO₃] (8)**

0.203 g (0.264 mmol) ReAA, 0.135 g (0.792 mmol) AgNO₃, 0.112 g (0.294 mmol) L8. Yield: 0.0609 g (0.0896 mmol, 34%). Elemental analysis for C₂₂H₁₆N₅O₇SRe: Calculated: C = 38.82 %, N = 10.29 %, S = 4.71 %, H = 2.37 %; Found: C = 38.85 %, N = 10.27 %, S = 4.69 %, H = 2.38 %. IR (ATR, cm^{-1}): $\nu_{\text{N-H}} = 3066$, $\nu_{\text{O-H}} = 2923, 2865$, $\nu_{\text{C=O}} = 2025, 1904, 1894$, $\nu_{\text{C=N}} = 1617$, $\nu_{\text{C=C}} = 1586, 1545$, $\nu_{\text{C-S}} = 806$. ^1H NMR (400 MHz, DMSO- d_6): δ 14.1 (1H, s), 9.4 (2H, d, $J = 4.9$ Hz), 9.1 (2H, broad multiplet), 8.1 (2H, broad doublet, $J = 19.8$ Hz), 7.6 (1H, s), 2.4 (3H, s), 2.2 (3H, s) ppm. $^{13}\text{C}\{^1\text{H}\}$ NMR (101 MHz, DMSO- d_6): δ 197.9, 190.0, 151.7, 148.7, 137.0, 134.8, 133.2,

132.9, 130.3, 127.8, 126.9, 13.8, 13.5 ppm. UV/Vis (DMSO): $\lambda_{\text{max}} = 341 \text{ nm}$, $\epsilon = 6\,340 \text{ M}^{-1} \text{ cm}^{-1}$. ESI-MS (CH₃OH, +ve ion mode): m/z 601.1 ([M - NO₃⁻ - H₂O]⁺); calcd, 600.6).

Stability Study

The stability of the complexes in DMSO, aqueous buffer and FBS solutions was monitored using time dependent UV/Vis absorption measurements. Briefly, the concentration of each complex was maintained at 10 μM except for complex 7. In fact, due to poor solubility, we used 5 μM concentration for compound 7. A 1:20 v/v DMSO: 10 mM phosphate buffer pH 7.4 in presence of 4 mM NaCl solution of the complexes was used to evaluate the aqueous solution stability. In case of the stability in FBS solution, we prepared the complex solution in 1:99 v/v DMSO: 10 mM phosphate buffer pH 7.4 in presence of 10% FBS. The stability of the complexes in solution was monitored up to 6 hours.

Determination of Acid dissociation constant (*pKa*)

pH measurements were performed using a Hanna pH211 Microprocessor pH meter, equipped with a HI 1131 probe, which was calibrated using standard buffer solutions, with pH = 4.01, 7.00, and 10.00. A Varian Cary 50 Conc UV/Vis spectrophotometer, coupled to a personal computer capable of performing least squares analyses on the absorption values vs pH data was utilised for the kinetic measurements. Microsoft Office Excel (2019) and Scientist Micromath, version 2.01 were used to fit the collected data to specific functions.^{88,89} A circulating water bath system was used to control and maintain the temperature at 25 °C. The ionic strength (μ) of all solutions was maintained at 1 M NaClO₄.

The stability of complexes in DMSO solution was also monitored by ESI-MS measurement. Briefly, 10 μM DMSO solution of the complexes were incubated for 48 hours at 37°C. Finally, 10 μL DMSO solution was diluted in 1 mL of methanol and analysed by ESI-MS.

Distribution Coefficient

The distribution coefficient or lipophilicity ($\log D$) was determined using standard shake flask technique.⁵⁸ Briefly, 40 μL 1 mM DMSO solution of complex was added to the pre-equilibrated 4 mL 10 mM phosphate buffer (pH 7.4) octanol mixture (1:1 v/v) and agitated continuously in a vertical shaker for 6 hours. Then, each layer of the mixture was separated by centrifugation and transferred to new vials. Further, the complex concentration in each layer was determined by measuring their absorption spectra. Finally, the lipophilicity was determined using equation 3 below.

$$\log D = \log \frac{C_{org}}{C_{aq}} \quad \text{Equation 3}$$

BSA binding study

The BSA binding study was performed by measuring the internal fluorescence quenching of BSA. The BSA has an intrinsic fluorescence emission maxima at 341 nm upon excitation at 280 nm.^{66,67} Briefly, 20 μM of BSA solution in 1X Tris buffer (pH 7.4) was incubated with different concentrations (0-10 equivalents) of complex solution for 15 min at 37°C. Further, their fluorescence intensities were recorded at 341 nm upon excitation at 280 nm. Finally, the fluorescence quenching constant and the binding constant were calculated using the Stern–Volmer equation (equation 4) and the Scatchard equation (equation 5) respectively.

$$\frac{F_0}{F} = 1 + K_{sv}[Q] \quad \text{Equation 4}$$

$$\log \frac{(F_0 - F)}{F} = \log K_a + n \log [Q] \quad \text{Equation 5}$$

In the equations, the fluorescence emission intensity of native protein is denoted as F_0 , the fluorescence emission intensity in presence of quencher is denoted as F , $[Q]$ corresponds to the concentration of quencher for F , K_{sv} is the Stern–Volmer quenching constant, K_a is denoted as the binding constant of quencher and protein, and n is the number of binding sites per protein molecule. Complexes showed no emission at 341 nm when excited at 280 nm.

DNA binding study

With model nucleobase

The DNA binding ability of complex **6** through covalent bond formation was studied in presence of a model nucleobase, Guanosine using ^1H NMR and ESI-MS. Precisely, 1.5 mM DMF- d_7 solution of complex **6** was allowed to react with 3 mM Guanosine solution in DMF- d_7 at 37°C and the binding was monitored at different interval of time by recording ^1H NMR spectra up to 24 hours. Finally, after 24 hours, 5 μL of DMF solution was diluted in 1 mL of methanol and analysed by ESI-MS.

Preparation of ctDNA solution

Calf thymus deoxyribonucleic acid (ctDNA) and tris-HCl buffer solution ($\text{pH} = 7.4$, 1M) were purchased from Sigma Aldrich, South Africa and used without further purification. The ctDNA stock solution was prepared by stirring a solution of ctDNA in tris-HCl buffer for 12 hours at room temperature. The purity of the stock solution was confirmed by the ratio of $A_{260\text{nm}}/A_{280\text{nm}}$ (1.843) indicating that the solution was free of protein.^{45,81,90,92} This solution was stored at 4°C between scans and discarded 2 days after preparation. The molar extinction coefficient value of ctDNA at 260 nm ($6600 \text{ Lmol}^{-1}\text{cm}^{-1}$) was employed in the determination of the stock solution concentration.

Ethidium Bromide displacement assay

To check the possibility of DNA intercalation due to the presence of a planer fused ring ligand system, we performed the standard ethidium bromide (EB) displacement assay. Precisely, 10 μM ctDNA solution in 1X Tris.NaCl buffer was incubated at 37°C with 3 equivalents of EB for 30 min. Followed by, 0 to 10 equivalents of complex **6** were added to the solution and incubated for additional 30 min at 37°C. Each solution was excited at 540 nm and emission was measured from 550 to 800 nm. Finally, the apparent binding constant (K_{app}) was measured using the equation 6.

$$K_{\text{EB}}[\text{EB}] = K_{\text{app}}[\text{C}_{50}] \quad \text{Equation 6}$$

Where, [EB] is the concentration of EB (30.0 μM), [C_{50}] is the concentration of complex when the reduction of fluorescence reach at 50%. K_{EB} is the binding constant of EB ($K_{\text{EB}} = 1 \times 10^7 \text{ M}^{-1}$ for ctDNA)⁹¹ The IC_{50} values were calculated from plots of normalized fluorescent intensity versus complex concentration (SI, Figure S24B).

DNA melting

The DNA binding ability of complex **6** were confirmed by measuring the DNA melting temperature prior to complex binding. Briefly, 40 μM of ctDNA was incubated with 30 μM of complex at 37°C for 15 min. Followed by the absorbance of the solution was measured at 260 nm in each °C increment in temperature within the range from 60°C - 97°C. A Cary UV 300, Agilent technologies was used to measure all absorbances. The experiment was programmed with 1°C/min temperature ramp rate from temperature range 60°C - 97°C and the holding time was 1 min. Finally, the absorbance of each experiment was normalised to 0 and 1, further compared with the melting temperature of native ctDNA.

Cell lines and cell culture

Human prostate adenocarcinoma (PC3) and normal human retinal pigment epithelial-1 (RPE-1) cells were originally procured from the American Type Culture Collection ATCC. The PC3 and RPE-1 cells were maintained in Ham's F-12K (Kaighn's) Medium and DMEM/F-12, GlutaMAX™ Supplement medium containing 10% fetal bovine serum (GIBCO) and 1% Penicillin-Streptomycin (100 units/mL, GIBCO) respectively.

Cytotoxicity

The standard Resazurin assay was performed to determine the cytotoxicity of the synthesized complexes. In particular, 4×10^3 cells were seeded in each well of a 96 well microplate and incubated at 37 °C under normoxic conditions (~15 % O₂ level). After 24 hours of the initial incubation period, the medium was replenished by a fresh metal complex-containing medium (100 μL/well) and incubated for an additional 48 hours. Initially, the metal complex was dissolved in DMSO and the target concentration was achieved by further dilution with the medium. A total of seven or nine different concentrations of the metal complex solutions from 10 nM to 100 μM were used to observe the dose dependent cytotoxicity. The ultimate concentration of DMSO in each well was ≤ 1 %. Finally, the metal complex-containing medium was carefully aspirated and an equal volume of Resazurin (0.2 mg/mL)-containing medium was added. After 4 hours of incubation at 37 °C, the fluorescence of the produced resorufin product ($\lambda_{\text{ex}} = 540$ nm, $\lambda_{\text{em}} = 590$ nm) was measured in either a Tecan infinite F200PRO Microplate Reader or a Cytation 5, Cell Imaging Multi-Mode Reader, BioTek. Finally, the half-maximal inhibitory concentration (IC₅₀) value was calculated using the GraphPad Prism software from the plot of % of cell viability vs log [complex concentration] after applying nonlinear fitting. Each of the reported IC₅₀ values are the mean of three individual experiments with standard deviation, and each concentration was assayed in sextuplicate in each successive experiment.

The cytotoxic inactivation of most selective complexes **3** and **6** in hypoxic condition (2.0 % O₂) were also measured against PC3 cells. A similar protocol as stated in normoxia cytotoxicity was followed to determine their IC₅₀ in hypoxic condition keeping everything unaltered except the incubation in presence of 2.0 % O₂. Initially, at least three consecutive cell passages were maintained in hypoxic condition before start any experiments.

Cytotoxicity against 3D cell spheroid

1 × 10⁴ PC3 cells were seeded in each well of a Corning™ 96 Well Ultra-Low Attachment Treated Spheroid Microplate. After 96 hours of incubation at 37°C in normoxic condition, the average spheroid size observed was 435 μm. Half of the medium was replaced by equal volume of complex-containing (two times of target concentrations) medium. After 72 hours, the cell viability was measured using AlamarBlue assay. Finally, the IC₅₀ values were determined by using GraphPad Prism software after applying four parameter fitting.

Intracellular accumulation study

The fluorescence property is highly dependent on pH and cellular micro environment.^{74,92} Hence, we quantified Re in different cellular organelles using ICP-MS to determine the complex localization in cells.

An adequate number of PC3 cells was seeded in a 150 mm diameter petri dish using F12K medium and incubated in normoxic conditions at 37 °C. The medium from each petri-dish was replenished every 2 days. When the cell confluency was reached around 80 - 90%, a fresh medium containing 5 μM of complexes **3** or **6** was added and incubated for an additional 1.5 hours in normoxic conditions at 37 °C. Cells were harvested by trypsinisation. The medium was removed by centrifugation and the cell pellet was washed twice with cold DPBS. The nucleus and mitochondria of treated cells were then isolated using the standard kit protocols mentioned below.

To determine the total rhenium uptake, 5×10^5 cells were collected and digested using 100 μL of 70% nitric acid at 60 °C for 12 hours. The acid solution was further diluted using 4900 μL of MilliQ water. Finally, the rhenium concentration was measured using ICP-MS. Each experiment was performed in triplicate.

Nuclei: The nuclei isolation kit, Nuclei EZ Prep (NUC101), Sigma-Aldrich, was used to isolate the nuclei from the complex-treated cells and the standard kit protocol was employed for the isolation process. The complex treated cells were exposed to 4 ml of ice-cold Nuclei EZ lysis buffer and vortex briefly to lyse the cells. The solution was settled at 4 °C for another 5 minutes and centrifuged at $500 \times g$ for 5 min at 4 °C. The supernatant was removed carefully. The cell and nuclei pellet were redissolved using ice-cold Nuclei EZ lysis buffer and the same process was repeated to maximise the nuclei yield. During this isolation step, both the nucleus and cells were stained with the trypan blue dye prior to counting using a haemocytometer to obtain the exact number of the nuclei and intact cells.

Mitochondria: The mitochondria isolation kit (MITOISO2), Sigma-Aldrich, was used to isolate the mitochondria from the complex-treated cells and the standard kit protocol was employed for the isolation procedures. By following the kit protocol, the complex treated cells were lysed using 1X extraction buffer at 4 °C using a Dounce homogenizer. The exact number of lysed cells was counted using a haemocytometer after trypan blue staining. The intact cells and other heavier cell fragments were removed from the solution by centrifugation at $600 \times g$ for 10 min at 4 °C. The supernatant was transferred carefully and centrifuged at 11000 (G) for 10 min at 4 °C to isolate the mitochondria. Hence, the total amount of isolated mitochondria corresponds to the total lysed cells. The percentage of rhenium accumulation in the nucleus and mitochondria was calculated using the total accumulated rhenium corresponding to 5×10^5 cells.

Sample preparation for ICP-MS

The samples were digested in either a 100 μL (cell pellet) or a 500 μL (nucleus and mitochondria pellet) of 70 % HNO_3 at 60 $^\circ\text{C}$ for 12 hours. The acid solution was further diluted (1:50 v/v) with MilliQ water. Finally, the rhenium concentration in the solution was analysed using a high resolution ICP-MS of ThermoScientific (Element II, ThermoScientific) instrument at the Institut de Physique du Globe de Paris, France.

Cellular Uptake Pathways

1.5×10^6 PC3 cells were seeded in a 6 cm petridish and incubated in normoxic condition at 37 $^\circ\text{C}$. After 24 hours of seeding, the cells were treated with different cellular uptake pathways inhibitors for 2 hours in normoxic condition. The inhibitor used here were: 1 mM tetraethylammonium chloride (cationic transporter inhibitor), 5 μM oligomycin and 50 mM 2-Deoxy-D-glucose (metabolic inhibitors), and 50 mM ammonium chloride (endocytotic inhibitor) as different uptake pathways inhibitors. Additionally, we pre-incubated the cells at 4 $^\circ\text{C}$ for 2 hours to determine the involvement of passive transport on cellular uptake process. After 2 hours, cells were washed twice with DPBS and 5 μM of complex (**3** and **6**) solution was added. After 2 h of incubation in normoxic condition, cells were harvested using trypsinisation and counted. 1×10^6 cells were separated and digested in 100 μL of conc. HNO_3 . Finally, the acid solution was diluted by addition of 4900 μL MQ water to keep the acid % within 2. The rhenium concentration in solution was measured by ICP-MS. Each successive experiment and control experiments were performed in three times to determine the average value with standard deviation.

Mito Stress Test using Seahorse apparatus

3×10^4 PC3 cells/well were seeded of a Seahorse XF Cell Culture Microplate using 80 μL of FBS supplemented F12K medium and incubated in normoxic condition for 24 hours at 37 $^\circ\text{C}$.

The medium was replaced by equal volume of compound (**3**; 0.4 and 5 μM , **6**; 0.05 and 2 μM , and cisplatin; 7 and 30 μM) containing medium. After 24h of treatment, media was removed, and the treated cells were washed very carefully with the Seahorse XF medium three times. Finally, the cells were incubated at 37°C for one hour in a non-CO₂ incubator. The Mito Stress assay was run in a Seahorse Xfe96 instrument, Agilent at 37°C using multiple inhibitors viz., ATP synthase inhibitor (oligomycin, 1 μM), proton gradient and mitochondrial membrane potential collapsing agent (FCCP, 1 μM), mitochondrial respiratory complex I and III inhibitor (rotenone, 1 μM and antimycin A, 1 μM respectively). After the experiment, the cells were fixed using 4% *p*-formaldehyde solution and stained the nucleus with DAPI. Each well was imaged in Cytation 5 Cell Imaging Multimode Reader, BioTek using a 10X objective lens. Finally, the cells from each images were calculated by using Gen5 software (SI, Figure S35) and by utilising the cell count and the data was normalised against same cell number.

Cell death mechanism

To evaluate the possible cell death pathways, we measured the cell viability in presence of different cell death pathway inhibitors.^{44,75} Briefly, 1×10^3 PC3 cells/well were seeded in 96-well plate and incubated for 24 hours in normoxic condition at 37 °C. The medium was removed and treated with inhibitors for 1 hour. Autophagy inhibitor: 3-Methyladenine (100 μM), apoptosis inhibitor: Z-VAD-FMK (20 μM), paraptosis inhibitor: cycloheximide (0.1 μM), and necrosis inhibitor: necrostatin-1 (60 μM) are the different inhibitors were used. After 1 hour, the inhibitor containing medium was removed and washed with 1X DPBS. Then, different concentrations of complex solution were added, and incubated for 36 hours in normoxic condition. Finally, the cell viability was determined by resazurin assay (check section “Cytotoxicity” for details) to evaluate the IC₅₀ values.

Annexin-V/PI assay for apoptosis detection

1.5×10^6 PC3 cells were seeded in a 6 cm petri-dish using a F12K medium and incubated at 37 °C in normoxic conditions. After 24 hours of incubation, the medium was replenished with a complex-containing medium and incubated additionally for 24 hours. Two different concentrations of complexes **3** and **6** were used to determine the possible apoptosis pathways for cell killing. The cells were then harvested by trypsinisation and washed twice with DPBS. The cells were further stained with both FITC tagged Annexin-V (cat. No. 556419, BD Biosciences) and propidium iodide (cat. No. 51-66211E, BD Biosciences). Finally, the stained cells were analysed using a BD™ LSR II flow cytometry instrument, BD Biosciences at Institut Curie, Paris, France.

ROS Analysis

1.5×10^4 PC3 cells were seeded in dark 96-well plate for 24 h. Four different concentrations of complexes **3** and **6** were used to treat the cells for 8 hours, and then, two different concentrations of H₂O₂ were used to treat the cells for 30 min (10 and 15 μM). The medium was removed, 40 μM DCFH-DiOxy-Q (Kit No. ab238535, Abcam) in 10% FBS containing HEPES was added in each well followed by incubation at 37 °C for 30 min. The cells were washed twice with HEPES and finally fluorescence intensity was measured (Eex/Eem; 485/530 nm) using Cytation 5 Cell Imaging Multimode Reader, BioTek. Then, the cells were fixed using *p*-formaldehyde and stained using DAPI. The cells were finally counted in the same way as stated before and utilised to normalize the data.

ASSOCIATED CONTENT

Supporting information

Supplementary file with additional information (PDF). The supplementary file contains crystallographic data (Table S1-S3) and interactions (Fig. S1-S6), stability study (Fig. S7-S14), pK_a determination (Fig. S15-S18), DNA binding study (Fig. S19-S24), BSA binding (Fig. S25-S28), cytotoxicity (Table S4 and Fig. S29-S33), mitochondrial respiration test (Fig. S34-S37), 1H NMR spectra (Fig. S38-S45), FT-IR spectra of complexes (Figs. S46-S53).

Accession codes

CCDC 2194247 contains the supplementary crystallographic data for this paper. The data can be obtained free of charge via www.ccdc.cam.ac.uk/data_request/cif, or by emailing data_request@ccdc.cam.ac.uk, or by contacting The Cambridge Crystallographic Data Centre, 12 Union Road, Cambridge CB2 1EZ, UK; fax: +44 1223 336033.

AUTHOR INFORMATION

Corresponding Authors

* Hendrik Visser, University of the Free State, Department of Chemistry, South Africa.
visserhg@ufs.ac.za

* Gilles Gasser, Chimie ParisTech, PSL University, CNRS, Institute of Chemistry for Life and Health Sciences, Laboratory for Inorganic Chemical Biology, France.
gilles.gasser@chimieparistech.psl.eu, www.gassergroup.com

* Marietjie Schutte-Smith, University of the Free State, Department of Chemistry, South Africa.
schuttem@ufs.ac.za

Author Contributions

The manuscript was written through contributions of all authors. All authors have given approval to the final version of the manuscript. Lucy Ellen Kapp: Writing - original draft, Investigation. Kallol Purkait: Investigation, Writing - original draft. Maria Dalla Pozza: investigation, writing. Gilles Gasser: Supervision, Writing - review & editing. Hendrik Gideon Visser: Supervision, Writing -review & editing. Marietjie Schutte-Smith: Funding acquisition, Project administration, Writing -review & editing, Conceptualization.

Funding Sources

Financial assistance from the University of the Free State is gratefully acknowledged. This work is based on research supported in part by the National Research Foundation of South Africa, unique grant number 116246. The intracellular accumulation study was financially supported by the European Union's Horizon 2020 research and innovation programme (Marie Skłodowska-Curie Innovative Training Network Nature-ETN, H2020-MSCA-ITN-2019-861381) and ERC Consolidator Grant PhotoMedMet to G.G. (GA 681679), by the ITMO Cancer AVIESAN (Alliance Nationale pour les Sciences de la Vie et de la Sante/ National Alliance for Life Sciences & Health) within the framework of the Cancer Plan (G.G) and has received support under the program “Investissements d’ Avenir” launched by the French Government and implemented by the ANR with the reference ANR-10-IDEX-0001-02 PSL (G.G.).

ACKNOWLEDGMENT

This work is based on research supported in part by the National Research Foundation of South Africa (Unique Grant no: 116246). The Grant holder acknowledges that opinions, findings and conclusions or recommendations expressed in any publication generated by the NRF supported research are that of the author(s) and that the NRF accepts no liability whatsoever in this regard. We sincerely acknowledge Mr. Pierre Burckel, Institut de Physique du Globe de Paris, for his kind

help regarding all the ICP-MS measurements and Mr. Francois Jacobs for the crystal data collection.

REFERENCES

¹ Kirgan, R. A.; Sullivan, B. P.; Rillema, D. P. *Topics in Current Chemistry*, 281st ed.; Balzani, V., Campagna, S., Eds.; Springer-Verlag.: Berlin, Heidelberg, 2007.

² Kalyanasundaram, K. *Photochemistry of Polypyridine and Porphyrin Complexes*, London ; San Diego : Academic Press, 1992 .

³ Arakawa, H.; Aresta, M.; Armor, J. N.; Barteau, M. A.; Beckman, E. J.; Bell, A. T.; Bercaw, J. E.; Creutz, X. C.; Dinjus, O. E.; Dixon, D. A.; Domen, K.; Dubois, D. L.; Eckert, J.; Fujita, E.; Gibson, O. D. H.; Goddard, W. A.; Goodman, D. W.; Keller, J.; Kubas, G. J.; Kung, H. H.; Lyons, J. E.; Manzer, L. E.; Marks, T. J.; Morokuma, K.; Nicholas, K. M.; Periana, R.; Que, L.; Rostrup-nielson, J.; Sachtler, W. M. H.; Schmidt, L. D.; Sen, A.; Somorjai, G. A.; Stair, P. C.; Stults, B. R.; Tumas, W. Catalysis Research of Relevance to Carbon Management : Progress , Challenges, and Opportunities. *Chem Rev.* **2001**, *101*, 953-996. <https://doi.org/10.1021/cr000018s>.

⁴ Morris, A. J.; Meyer, G. J.; Fujita, E. Molecular Approaches to the Photocatalytic Reduction of Carbon Dioxide for Solar Fuels. *Acc. Chem. Res.* **2009**, *42* (12), 1983-1994.

⁵ Benson, E.E.; Kubiak, C.P.; Sathrum, A.J.; Smieja, J.M. 2009 Renewable Energy Issue Energy Research to Liquid Fuels W. *Chem. Soc. Rev.* **2009**, *38*, 89-99.

⁶ Balzani, V.; Schoonover, J. R.; Scandola, F. *Inorganic Chemistry: Molecular Level Artificial Photosynthetic Materials*, 44th ed.; Meyer, G. J., Ed.; John Wiley & Sons Inc.: New York, 1997.

⁷ Balzani, V.; Scandola, F. *Supramolecular Photochemistry*, V.; Kemp, T. J., Ed.; Ellis Horwood: London, 1991.

⁸ Grätzel, M. Solar Energy Conversion by Dye-Sensitized Photovoltaic Cells. *Inorg. Chem.* **2005**, *44*, 6841-6851. <https://doi.org/10.1021/ic0508371>.

⁹ Nazeeruddin, M. K.; Grätzel, M. *Semiconductor Photochemistry and Photophysics*; Ramamurthy, V., Schanze, K. S., Eds.; Marcel Dekker Inc.: New York, 2003. 10.1201/9780203912294

¹⁰ Keene, F. R.; Sullivan, B. P. *Electrochemical and Electrocatalytic Reactions of Carbon Dioxide*; Sullivan, B. P., Krist, H. E., Guard, H. E., Eds.; Elsevier: Amsterdam, 1992. 10.1524/zpch.1995.189.part_2.278

¹¹ Lo, K. K.; Ng, D. C.; Hui, W.; Cheung, K. Isothiocyanate Moiety – Versatile Labelling Reagents for Biomolecules. *J. Chem. Soc., Dalton Trans.* **2001**, 3, 2634-2640. <https://doi.org/10.1039/b103371a>.

¹² Amoroso, A. J.; Arthur, R. J.; Coogan, M. P.; Hayes, A. J.; Court, J. B.; Ferna, V.; Lloyd, D.; Millet, C.; Pope, S. J. A. A. Thiol-Reactive Luminophore for Fluorescence Microscopy Accumulates in Mitochondria w Z. *New J. Chem.* **2008**, 32, 1097-1102. <https://doi.org/10.1039/b802215a>.

¹³ Gasser, G.; Ott, I.; Metzler-nolte, N. Organometallic Anticancer Compounds. *J. Med. Chem. Perspect.* **2011**, 54, 3-25. <https://doi.org/10.1021/jm100020w>.

¹⁴ Hartinger, C. G.; Metzler-nolte, N.; Dyson, P. J. Challenges and Opportunities in the Development of Organometallic Anticancer Drugs. *Organometallics* **2012**, 31, 5677-5685.

¹⁵ Gasser, G.; Metzler-nolte, N. The Potential of Organometallic Complexes in Medicinal Chemistry. *Curr. Opin. Chem. Biol.* **2012**, 16, 84-91. <https://doi.org/10.1016/j.cbpa.2012.01.013>.

¹⁶ Bruijninx, P. C. A.; Sadler, P. J. New Trends for Metal Complexes with Anticancer Activity. *Curr. Opin. Chem. Biol.* **2008**, 12, 197-206. <https://doi.org/10.1016/j.cbpa.2007.11.013>.

¹⁷ Hartinger, C. G.; Dyson, P. J. Bioorganometallic Chemistry — from Teaching Paradigms to Medicinal Applications. *Chem. Soc. Rev.* **2009**, 38, 391-401. <https://doi.org/10.1039/b707077m>.

¹⁸ Slikboer, S. R.; Pitchumony, T. S.; Banevicius, L.; Mercanti, N.; Edem, P. E.; Valliant, J. F. Imidazole Fused Phenanthroline (PIP) Ligands for the Preparation of Multimodal Re(i) and ^{99m}Tc(i) Probes. *Dalt. Trans.* **2020**, 49 (42), 14826–14836. <https://doi.org/10.1039/d0dt02829k>.

¹⁹ Qasim, S. S.; Ali, S. S.; Ahmed, S. K.; June, A. Research Journal of Pharmaceutical, Biological and Chemical. *Res. J. Pharm. Biol. Chem. Sci.* **2011**, 2 (2), 423-428.

²⁰ Jayabharathi, J.; Thanikachalam, V.; Perumal, M. V. A Study on the Binding Interaction between the Imidazole Derivative and Bovine Serum Albumin by Fluorescence Spectroscopy. *J. Lumin.* **2012**, 132 (3), 707–712. <https://doi.org/10.1016/j.jlumin.2011.10.023>.

²¹ Gomleksiz, M.; Alkan, C.; Erdem, B. Synthesis, Characterization and Antibacterial Activity of Imidazole Derivatives of 1,10-Phenanthroline and Their Cu(II), Co(II) and Ni(II) Complexes. *S. Afr. J. Chem.* **2013**, 66, 107-112.

²² Chao, H.; Li, R.; Ye, B.; Li, H.; Feng, X.; Cai, J.; Zhou, J.; Ji, L. Syntheses, Characterization and Third Order Non-Linear Optical Properties of the Ruthenium. *J. Chem. Soc., Dalt. Trans.* **1999**, 3711-3717.

²³ Bonello, R. O.; Morgan, I. R.; Yeo, B. R.; Jones, L. E. J.; Benson, M.; Fallis, I. A.; Pope, S. J.A. ACSC. *J. Organomet. Chem.* **2013**, I. <https://doi.org/10.1016/j.jorganchem.2013.08.031>.

²⁴ Rafique, S.; Idrees, M.; Nasim, A.; Akbar, H.; Athar, A. Transition Metal Complexes as Potential Therapeutic Agents. *Mol. Biol.* **2010**, 5 (April), 38-45.

²⁵ Shaheen, F.; Badshah, A.; Gielen, M.; Dusek, M.; Fejfarova, K.; Vos, D. De; Mirza, B. Synthesis , Characterization , Antibacterial and Cytotoxic Activity of New Palladium(II) Complexes with Dithiocarbamate Ligands: X-Ray Structure of Bis(Dibenzyl-1-S :S0-Dithiocarbamato) Pd(II). *J. Org. Chem.* **2007**, 692(3), 3019-3026. <https://doi.org/10.1016/j.jorganchem.2007.03.019>.

²⁶ Leonidova, A.; Gasser, G. Underestimated Potential of Organometallic Rhenium Complexes as Anticancer Agents. *ACS Chem. Biol.* **2014**, 9(10), 2180-2193. <https://doi.org/10.1021/cb500528c>.

²⁷ Liew, H. S.; Mai, C. W.; Zulkefeli, M.; Madheswaran, T.; Kiew, L. V.; Delsuc, N.; Lee Low, M. Recent Emergence of Rhenium(I) Tricarbonyl Complexes as Photosensitisers for Cancer Therapy. *Molecules* **2020**, 25(18), 1-23. <https://doi.org/10.3390/molecules25184176>.

²⁸ Pan, Z. Y.; Cai, D. H.; He, L. Dinuclear Phosphorescent Rhenium(i) Complexes as Potential Anticancer and Photodynamic Therapy Agents. *Dalton Trans.* **2020**, 49(33), 11583-11590. <https://doi.org/10.1039/d0dt02424d>.

²⁹ Capper, M. S.; Packman, H.; Rehkämper, M. Rhenium-Based Complexes and in Vivo Testing: A Brief History. *ChemBioChem* **2020**, 21(15), 2111-2115. <https://doi.org/10.1002/cbic.202000117>.

³⁰ Bauer, E.B.; Haase, A.A.; Reich, R.M.; Crans, D.C.; Kühn, F.E. Organometallic and coordination rhenium compounds and their potential in cancer therapy. *Coord. Chem. Rev.* **2019**, 393, 79. <https://doi.org/10.1016/j.ccr.2019.04.014>.

³¹ Collery, P.; Desmaele, D.; Vijaykumar, V. Design of Rhenium Compounds in Targeted Anticancer Therapeutics. *Curr. Pharm. Des.* **2019**, 25(31), 3306-3322. doi: 10.2174/1381612825666190902161400.

³² Wang, F. X.; Liang, J. H.; Zhang, H.; Wang, Z. H.; Wan, Q.; Tan, C. P.; Ji, L. N.; Mao, Z. W. Mitochondria-Accumulating Rhenium(I) Tricarbonyl Complexes Induce Cell Death via Irreversible Oxidative Stress and Glutathione Metabolism Disturbance. *ACS Appl. Mater. Interfaces* **2019**, 11(14), 13123-13133. <https://doi.org/10.1021/acsami.9b01057>.

³³ King, A.P.; Marker, S.C.; Swanda, R.V.; Woods, J.J.; Qian, S.-B.; Wilson, J.J. A Rhenium Isonitrile Complex Induces Unfolded Protein Response-Mediated Apoptosis in Cancer Cells. *Chem. Eur. J.* **2019**, 25, 9206–9210. doi: 10.1002/chem.201902223.

³⁴ Marker S.C.; King, A.P.; Granja, S.; Vaughn, B.; Woods, J.J.; Boros, E.; Wilson, J.J. Exploring the In Vivo and In Vitro Anticancer Activity of Rhenium Isonitrile Complexes. *Inorg Chem.* **2020**, 59(14), 10285-10303. doi: 10.1021/acs.inorgchem.0c01442.

³⁵ Neuditschko, B.; King, A.P.; Huang, A.; Janker, L.; Bileck, A.; Borutzki, Y.; Marker, S.C.; Gerner, C.; Wilson, J.J.; Meier-Menches, S.M. An Anticancer Rhenium Tricarbonyl Targets Fe-S Cluster Biogenesis in Ovarian Cancer Cells. *Angew. Chem. Int. Ed.* **2022**, 61(43), e202209136. doi.org/10.1002/anie.202209136.

³⁶ Simpson, P. V.; Falasca, M.; Massi, M. Properties and Prospects for Rhenium(i) Tricarbonyl N-Heterocyclic Carbene Complexes. *Chem. Commun.* **2018**, 54(88), 12429-12438. <https://doi.org/10.1039/c8cc06596a>.

³⁷ Delasoie, J.; Pavic, A.; Voutier, N.; Vojnovic, S.; Crochet, A.; Nikodinovic-Runic, J.; Zobi, F. Identification of Novel Potent and Non-Toxic Anticancer, Anti-Angiogenic and Antimetastatic Rhenium Complexes against Colorectal Carcinoma. *Eur. J. Med. Chem.* **2020**, 204, 112583. <https://doi.org/10.1016/j.ejmech.2020.112583>.

³⁸ Ye, R. R.; Tan, C. P.; Lin, Y. N.; Ji, L. N.; Mao, Z. W. A Phosphorescent Rhenium(I) Histone Deacetylase Inhibitor: Mitochondrial Targeting and Paraptosis Induction. *Chem. Commun.* **2015**, 51(39), 8353-8356. <https://doi.org/10.1039/c5cc02354h>.

³⁹ Hanahan, D.; Weinberg, R. A. Review Hallmarks of Cancer : The Next Generation. *Cell* **2011**, 144(5), 646–674. <https://doi.org/10.1016/j.cell.2011.02.013>.

⁴⁰ Banerjee, S.; Li, Y.; Wang, Z.; Sarkar, F. H. Multi-Targeted Therapy of Cancer by Genistein. *Cancer Lett.* **2008**, 269, 226-242. <https://doi.org/10.1016/j.canlet.2008.03.052>.

⁴¹ Hu, S.; Ma, W.; Wang, Y.; Zhou, Z.; Zhang, R.; Du, K.; Zhang, H.; Sun, M.; Jiang, X.; Tu, H.; Tang, X.; Yoa, X.; Chen, P. Synthesis and anticancer evaluations of novel 1H-imidazole [4,5-f][1,10] phenanthroline derivative for the treatment of colorectal cancer. *Eur. J. Pharmacol.* **2022**, 928, 175120-. <https://doi.org/10.1016/j.ejphar.2022.175120>

⁴² Bai, M.; Liu, N.; Zhou, Y.; Liu, J.; Zou, J.; Tan, W.; Huang, X.; Mei, W. Synthesis of Fluorinated Imidazole[4,5f][1,10]phenanthroline Derivatives as Potential Inhibitors of Liver Cancer Cell Proliferation by Inducing Apoptosis via DNA Damage. *ChemMedChem.* **2021**, 17, e202100537. <https://doi.org/10.1002/cmdc.202100537>

⁴³ Ali, I.; Lone, M. N.; Aboul-Enein, H. Y. Imidazoles as Potential Anticancer Agents. *Medchemcomm* **2017**, 8 (9), 1742–1773. <https://doi.org/10.1039/c7md00067g>.

⁴⁴ Knopf, K.M.; Murphy, B.L.; MacMillan, S.N.; Baskin, J.M.; Barr, M.P.; Boros, E.; Wilson, J.J. In vitro anticancer activity and in vivo biodistribution of rhenium(I) tricarbonyl aqua complexes. *J. Am. Chem. Soc.* **2017**, 139, 40, 14302-14314.

⁴⁵ Alberto, R.; Egli, A.; Abram, U.; Hegetschweiler, C. K.; Gramlich, V.; Schubiger, P. A. Synthesis and Reactivity of [NEt₄]₂[ReBr₃(CO)₃]. Formation and Structural Characterization of the Clusters [NEt₄][Re₃(u-OH)₃(CO)₉] and [NEt₄][Re₂(u-OH)₃(CO)₆] by Alkaline Titration. *J. Chem. Soc. Dalton Trans.* **1994**, No. 1, 2815–2820. <https://doi.org/10.1039/DT9940002815>

⁴⁶ Hevia, E.; Pérez, J.; Riera, V.; Miguel, D.; Kassel, S.; Rheingold, A. New Synthetic Routes to Cationic Rhenium Tricarbonyl Bipyridine Complexes with Labile Ligands. *Inorg. Chem.* **2002**, *41*(18), 4673-4679. <https://doi.org/10.1021/ic020174c>.

⁴⁷ Hevia, E.; Pérez, J.; Riera, L.; Riera, V.; Miguel, D. Reactive Alkoxide Complexes of Groups 6 and 7 Metals. *Organometallics* **2002**, *21*(9), 1750-1752. <https://doi.org/10.1021/om010977s>.

⁴⁸ Hightower, S. E.; Corcoran, R. C.; Sullivan, B. P. Unusual, Bifurcated Photoreactivity of a Rhenium(I) Carbonyl Complex of Triethynylphosphine. *Inorg. Chem.* **2005**, *44*(26), 9601-9603. <https://doi.org/10.1021/ic050901e>.

⁴⁹ Domínguez, S. E.; Alborés, P.; Fagalde, F. Photoinduced Linkage Isomerization in New Rhenium(I) Tricarbonyl Complexes Coordinated to N-Nitrite and O-Nitrite. *Polyhedron* **2014**, *67*, 471-480. <https://doi.org/10.1016/j.poly.2013.10.002>.

⁵⁰ Kapp, L. E.; Schutte-Smith, M.; Twigge, L.; Visser, H. G. Synthesis, Characterization and DNA Binding of Four Imidazo[4,5-*f*]1,10-Phenanthroline Derivatives. *J. Mol. Struct.* **2022**, *1247*, 131235.

⁵¹ Schutte, M.; Visser, H. G. Aqua-Tricarbonyl(4-Carboxy-Pyridine-2-Carboxylato-K²N,O²)Rhenium(I). *Acta Crystallogr. Sect. E Struct. Reports Online* **2008**, *64*(10). <https://doi.org/10.1107/S160053680802761X>.

⁵² Schutte, M.; Visser, H. G.; Brink, A. Bromidotricarbonylrhenium(I). *Acta Crystallogr. Sect. E Struct. Reports Online* **2009**, *65*(12), 1320-1328. <https://doi.org/10.1107/S1600536809047242>.

⁵³ Schutte, M.; Visser, H. G.; Roodt, A. Tetra-Ethyl-Ammonium Bromidotricarbonyl(Tropolonato)Rhenate(I). *Acta Crystallogr. Sect. E Struct. Reports Online* **2010**, *66*(7). <https://doi.org/10.1107/S1600536810024505>.

⁵⁴ Vinck, R.; Gandioso, A.; Burckel, P.; Saubaméa, B.; Cariou, K.; Gasser, G. Red-Absorbing Ru(II) Polypyridyl Complexes with Biotin Targeting Spontaneously Assemble into Nanoparticles in Biological Media. *Inorg. Chem.* **2022**, *61*, 13576-13585. DOI: <https://doi.org/10.1021/acs.inorgchem.2c02214>

⁵⁵ Egli, A.; Hegetschweiler, K.; Alberto, R.; Abram, U.; Schibli, R.; Hedinger, R.; Gramlich, V.; Kissner, R.; Schubiger, P. A. Hydrolysis of the Organometallic Aqua Ion Fac-Triaquatricarbonylrhenium(I). Mechanism, PKa, and Formation Constants of the Polynuclear Hydrolysis Products. *Organometallics* **1997**, *16*(9), 1833-1840. <https://doi.org/10.1021/om960894p>.

⁵⁶ Schutte, M.; Roodt, A.; Visser, H. G. Coordinated Aqua vs Methanol Substitution Kinetics in *fac*-Re(I) Tricarbonyl Tropolonato Complexes. *Inorg. Chem.* **2012**, *51*(21), 11996-12006. <https://doi.org/10.1021/ic301891u>.

⁵⁷ Schutte-Smith, M.; Marker, S.C.; Wilson, J.J.; Visser, H.G. Aquation and Anation Kinetics of Rhenium(I) Dicarbonyl Complexes: Relation to Cell Toxicity and Bioavailability. *Inorg. Chem.* **2020**, *59*, 15888-15897. <https://dx.doi.org/10.1021/acs.inorgchem.0c02389>.

⁵⁸ Zhang, C.; Wang, Y.; Wang, F. Determination and temperature dependence of n-octanol/water partition coefficients for seven sulfonamides from (298.15 to 333.15) K. *Bull. Korean Chem. Soc.* **2007**, *28*(7), 1183-1186.

⁵⁹ Ye, R. R.; Tan, C. P.; Chen, M. H.; Hao, L.; Ji, L. N.; Mao, Z. W. Mono- and Dinuclear Phosphorescent Rhenium(I) Complexes: Impact of Subcellular Localization on Anticancer Mechanisms. *Chem. - A Eur. J.* **2016**, *22*(23), 7800-7809. <https://doi.org/10.1002/chem.201505160>.

⁶⁰ Sugio, S.; Kashima, A.; Mochizuki, S.; Noda, M.; Kobayashi, K. Crystal structure of human serum albumin at 2.5Å resolution. *Protein Eng.* **1999**, *12*(6), 439-446. doi: 10.1093/protein/12.6.439.

⁶¹ Fanali, G.; di Masi, A.; Trezza, V.; Marino, M.; Fasano, M.; Ascenzi, P. Human serum albumin: from bench to bedside. *Mol. Aspects Med.* **2012**, *33*(3), 209-290. doi: 10.1016/j.mam.2011.12.002.

⁶² Curry, S.; Mandelkow, H.; Brick, P.; Franks, N. Crystal structure of human serum albumin complexed with fatty acid reveals an asymmetric distribution of binding sites. *Nat. Struct. Biol.* **1998**, *5*(9), 827-835. doi: 10.1038/1869.

⁶³ Oettl, K.; Marsche, G. Redox state of human serum albumin in terms of cysteine-34 in health and disease. *Methods Enzymol.* **2010**, *474*, 181-195. doi: 10.1016/S0076-6879(10)74011-8.

⁶⁴ Karges, J.; Kalaj, M.; Gembicky, M.; Cohen, S.M. Re^I Tricarbonyl Complexes as Coordinate Covalent Inhibitors for the SARS-CoV-2 Main Cysteine Protease. *Angew. Chem. Int. Ed.* **2021**, *60*(19), 10716-10723. doi.org/10.1002/anie.202016768.

⁶⁵ Capper, M.S.; Carcia, A.E.; Macia, N.; Lai, B.; Lin, J.-B.; Nomura, M.; Alihosseinzadeh, A.; Ponnurangam, S.; Heyne, B.; Shemanko, C.S.; Jalilehvand, F. Cytotoxicity, cellular localization and photophysical properties of Re(I) tricarbonyl complexes bound to cysteine and its derivatives. *J. Biol. Inorg. Chem.* **2020**, *25*(5), 759-776. DOI: 10.1007/s00775-020-01798-9.

⁶⁶ Alagesan, M.; Sathyadevi, P.; Krishnamoorthy, P.; Bhuvanesh, N.S.P.; Dharmaraj, N. DMSO containing ruthenium(II) hydrazone complexes: in vitro evaluation of biomolecular interaction and anticancer activity. *Dalton Trans.* **2014**, *43*, 15829-15840

⁶⁷ Singh, N.; Kumar, N.; Rathee, G.; Sood, D.; Singh, A.; Tomar, V.; Dass, S.K.; Chandra, R. Privileged scaffold chalcone: synthesis, characterization and its mechanistic interaction studies with BSA employing spectroscopic and chemoinformatics approaches. *ACS Omega* **2020**, *5*, 2267-2279.

⁶⁸ Alanazi, A.M.; Abdelhameed, A.S.; Bakheit, A.H.; Darwish, I.A. Exploring the interaction forces involved in the binding of the multiple myeloma drug lenalidomide to bovine serum albumin. *J. Mol. Liq.* **2017**, *238*, 3-10. doi.org/10.1016/j.molliq.2017.04.110.

⁶⁹ Sulkowska, A.; Rownicka, J.; Bojko, B.; Sulkowski, W. Interaction of anticancer drugs with human and bovine serum albumin. *J. Mol. Struct.* **2003**, *651-653*, 133-140. doi.org/10.1016/S0022-2860(02)00642-7.

⁷⁰ Szkudlarek, A.; Wilk, M.; Maciazek-Jurczyk, M. In Vitro Investigations of Acetohexamide Binding to Glycated Serum Albumin in the Presence of Fatty Acid. *Molecules* **2020**, *25*(10), 2340. doi.org/10.3390/molecules25102340.

⁷¹ Yang, J.; Zhao, J. X.; Cao, Q.; Hao, L.; Zhou, D.; Gan, Z.; Ji, L. N.; Mao, Z. W. Simultaneously Inducing and Tracking Cancer Cell Metabolism Repression by Mitochondria-Immobilized Rhenium(I) Complex. *ACS Appl. Mater. Interfaces* **2017**, *9*(16), 13900-13912. https://doi.org/10.1021/acsami.7b01764.

⁷² Imstepf, S.; Pierroz, V.; Rubbiani, R.; Felber, M.; Fox, T.; Gasser, G.; Alberto, R. Organometallic Rhenium Complexes Divert Doxorubicin to the Mitochondria. *Angew. Chem. Int. Ed.* **2016**, *55*, 2792-2795. http://dx.doi.org/10.1002/anie.201511432.

⁷³ Imstepf, S.; Pierroz, V.; Raposinho, P.; Bauwens, M.; Felber, M.; Fox, T.; Shapiro, A.B.; Freudenberg, R.; Fernandes, C.; Gama, S.; Gasser, G.; Motthagy, F.; Santos, I.R.; Alberto, R. Nuclear Targeting with an Auger Electron Emitter Potentiates the Action of a Widely Used Antineoplastic Drug. *Bioconjugate Chem.* **2015**, *26*, 12, 2397-2407. https://doi.org/10.1021/acs.bioconjchem.5b00466.

⁷⁴ Konkankit, C.C.; King, A.P.; Knopf, K.M.; Southard, T.L.; Wilson, J.J. In Vivo Anticancer Activity of a Rhenium(I) Tricarbonyl Complex. *ACS Med. Chem. Lett.* **2019**, *10*(5), 822-827.

⁷⁵ Karges, J.; Kuang, S.; Maschietto, F.; Blacque, O.; Ciofini, I.; Chao, H.; Gasser, G. Rationally designed ruthenium complexes for 1- and 2- photon photodynamic therapy. *Nature Communications* **2020**, *11*, 3262. doi.org/10.1038/s41467-020-16993-0.

⁷⁶ Hao, Wenshan, Chang, C.-P. B.; Tsao, C.-C.; Xu, J. Oligomycin-induced Bioenergetic Adaptation in Cancer Cells with Heterogeneous Bioenergetic Organization. *J. Biol. Chem.* **2010**, 285(17), 12647-12654. DOI 10.1074/jbc.M109.084194.

⁷⁷ Zhang, D.; Li, J.; Wang, F.; Hu, J.; Wang, S.; Sun, Y. 2-Deoxy-D-glucose targeting of glucose metabolism in cancer cells as a potential therapy. *Cancer Letters* **2014**, 355, 176-183. <https://doi.org/10.1016/j.canlet.2014.09.003>.

⁷⁸ Dantuma, N.P.; Pijnenburg, M.A.P.; Diederens, J.H.B.; van der Horst, D.J. Developmental down-regulation of receptor-mediated endocytosis of an insect lipoprotein. *J. Lipid Res.* **1997**, 38, 254-265. [https://doi.org/10.1016/S0022-2275\(20\)37438-1](https://doi.org/10.1016/S0022-2275(20)37438-1).

⁷⁹ Dean, R.T.; Jessup, W.; Roberts, C.R. Effects of exogenous amines on mammalian cells, with particular reference to membrane flow. *Biochem. J.* **1984**, 217(1), 27-40. doi: 10.1042/bj2170027.

⁸⁰ Gillespie, E.J., Ho, C.-L.C.; Balaji, K.; Bradley, K.A. Selective inhibitor of endosomal trafficking pathways exploited by multiple toxins and viruses. *PNAS* **2013**, 110(50), E4904-E4912. <https://doi.org/10.1073/pnas.1302334110>.

⁸¹ Guan, R.; Chen, Y.; Zeng, L.; Rees, T.W.; Jin, C.; Huang, J.; Chen, Z.-S.; Ji, L.; Chao, H. Oncosis-inducing cyclometalated iridium(III) complexes. *Chem. Sci.* **2018**, 9, 5183-5190.

⁸² Bruker, SAINT-Plus, Version 7.12 (including XPREP), Bruker AXS Inc., Madison, Wisconsin, USA, 2004.

⁸³ A. Altomare, M. C. Burla, M. Camalli, G. L. Cascarano, C. Giacovazzo, A. Guagliardi, A. G. Moliterni, G. Polidori and R. Spagna, *J. Appl. Crystallogr.*, 1999, **32**, 115–119.

⁸⁴ G. M. Sheldrick, *Acta Crystallogr. Sect. A Found. Crystallogr.*, 2008, **64**, 112–122.

⁸⁵ L. J. Farrugia, *J. Appl. Crystallogr.*, 1999, **32**, 837–838.

⁸⁶ Diamond - Crystal and Molecular Structure Visualization, Crystal Impact, H. Putz & K. Brandenburg GbR, Kreuzherrenstr. 102, 53227 Bonn, Germany, 2022.

⁸⁷ Kapp, L.E.; Schutte-Smith, M.; Twigge, L.; Visser, H.G. Synthesis, characterization and DNA binding of four imidazo[4,5-*f*]1,10-phenanthroline derivatives. *J. Mol. Struct.* **2022**, *1247*, 131235.

⁸⁸ Microsoft Office. Microsoft Corporation 2019.

⁸⁹ MicroMath. Scientist. MicroMath Inc.: Salt Lake City, UT 1995.

⁹⁰ Sirajuddin, M.; Ali, S.; Badshah, A. Drug-DNA Interactions and Their Study by UV-Visible, Fluorescence Spectroscopies and Cyclic Voltametry. *J. Photochem. Photobiol. B Biol.* **2013**, *124*, 1-19. <https://doi.org/10.1016/j.jphotobiol.2013.03.013>.

⁹¹ Malina, J.; Hannon, M.J.; Brabec, V. DNA binding of dinuclear iron(II) metallosupramolecular cylinders. DNA unwinding and sequence preference. *Nucl. Acids Res.* **2008**, *36*, 3630-3638.

⁹² Gasser, G.; Neumann, S.; Ott, I.; Seitz, M.; Heumann, R.; Metzler-Nolte, N. Preparation and Biological Evaluation of Di-HeteroOrganometallic-Containing PNA Bioconjugates. *Eur. J. Inorg. Chem.* **2011**, *36*, 5471-5478.